

**Functionalisation of mesoporous materials for
application as additives in high temperature
PEM fuel cell membranes**

Von der Naturwissenschaftlichen Fakultät
der Gottfried Wilhelm Leibniz Universität Hannover

zur Erlangung des Grades

**Doktor der Naturwissenschaft
Dr. rer. nat.**

genehmigte Dissertation
von

Dipl.-Chem. Monir Sharifi

Geboren am 15.06.1983 in Kabul (Afghanistan)

2012

Referent: Prof. Dr. Michael Wark
Korreferent: Prof. Dr. Jürgen Caro
Tag der Promotion: 06.03.2012

Preface

The results of this thesis were achieved in the past three years during my work as a scientific assistant at the Institute of Physical Chemistry and Electrochemistry at the Gottfried Wilhelm Leibniz Universität Hannover and at the Department of Technical Chemistry at the Ruhr-Universität Bochum. The financial support was granted by the Deutsche Forschungsgemeinschaft (DFG) (WA 1116/15, SPP1181) under the guidance of Prof. Dr. Michael Wark and Prof. Dr. Jürgen Caro.

Six research articles are presented within this thesis. I am the first author in each of these papers. The following statement will point out my contributions to these articles. I would like to acknowledge the beneficial encouragement during the preparation of the manuscript from my co-authors, particularly by Prof. Dr. Michael Wark.

The first article in Chapter 2, *Proton conductivity of ordered mesoporous materials containing aluminium*, presents the synthesis of proton conducting mesoporous Si-MCM-41 modified with aluminium and was written by myself. The solid state ^{27}Al magic angle spinning nuclear magnetic resonance (MAS NMR) measurements and interpretation by Dr. Martin Wilkening is appreciated. Furthermore, I performed X-ray diffraction (XRD), energy-dispersive X-ray spectroscopy (EDXS), nitrogen adsorption, scanning electron microscopy (SEM) and impedance spectroscopy (IS). I acknowledge the fruitful discussions with all co-authors.

In Chapter 3 sulphonic acid functionalised Si-MCM-41 were investigated by small angle neutron scattering (SANS) and by MAS NMR measurements. Within this chapter, the first article, *Detection of homogeneous distribution of functional groups in mesoporous silica by small angle neutron scattering and in-situ adsorption of nitrogen or water*, was written by myself. I kindly thank Dr. Dirk Wallacher for the technical support and sample preparation during SANS measurements at the Berlin Helmholtz-Zentrum for Neutron Scattering. Dr. Michaela Wilhelm recorded the water adsorption isotherms. The SANS measurements were conducted by Prof. Dr. Michael Wark and me in equal shares. In addition, I performed the corresponding characterization by IS and gas adsorption measurements.

Prof. Dr. Dieter Freude and I mainly wrote the second article, *Highly proton conducting sulphonic acid functionalised mesoporous materials studied by impedance spectroscopy, MAS NMR spectroscopy and MAS PFG NMR diffusometry*, with kind support of the co-authors. All solid state NMR measurements, preparations and interpretations were performed by Prof. Dr. Dieter Freude. I synthesised the

proton conducting materials Si-MCM-41-SO₃H that were used for this study and investigated IS measurements including discussion.

The first article in Chapter 4, *Proton conductivity of SO₃H-functionalised benzene-PMO*, was written by Dr. Christof Köhler and me, with kind support of all co-authors. The characterization by XRD, SANS, gas adsorption and IS were performed and interpreted by me. Furthermore, I prepared the PMO materials presented in this article. All theoretical calculations and discussions were done by Dr. Pia Tölle and Dr. Christof Köhler.

The second article within this Chapter, *Small angle neutron scattering and in-situ adsorption of nitrogen study on periodic mesoporous organosilica materials*, was written with kind assistance of Prof. Dr. Michael Wark. All SANS experiments were done by Prof. Dr. Michael Wark and me in equal shares. Additionally all gas adsorption measurements were performed by me.

The formation of sulphonic acid groups by different oxidation methods is presented in the article, *Investigation on the optimal oxidation agent for a maximum yield of sulphonic*, within Chapter 5. Data interpretation as well as manuscript preparation was fully conducted by myself. The syntheses of all studied samples were done by Jenny Schneider under my supervision. I kindly acknowledge the cooperation with her.

Acknowledgement

It was a great pleasure for me, to work on the field of mesoporous materials for the application in fuel cell membranes. I would like to express my grateful appreciation to all of those, who supported me in any way during my research work.

First of all, I would like to deeply thank Prof. Dr. Michael Wark for his excellent and outstanding support during the entire thesis. Only due to his intensive support, I was able to publish my results in various journals. He offered me the possibility to get insights into many different areas of research work.

I am especially grateful to Prof. Dr. Jürgen Caro, who gave me the opportunity to work in his working group on my Ph.D. thesis at the Institute of Physical Chemistry and Electrochemistry at the Gottfried Wilhelm Leibniz Universität Hannover.

Furthermore I would like to thank Prof. Dr. Josef-Christian Buhl from the Institute of Mineralogy at the Gottfried Wilhelm Leibniz Universität Hannover for his willingness as third examiner.

I also thank my collaboration and project partners, namely, Prof. Dr. Dieter Freude, Dr. Christof Köhler, Dr. Pia Tölle, Dr. Dirk Wallacher and Dr. Martin Wilkening.

I would also like to express my gratitude to all members of Physical Chemistry and Electrochemistry, particularly Florian Bittner, Konstantin Efimov, Tobias Klande, Oliver Merka and Frank Steinbach for their helpful input regarding my thesis and the nice atmosphere at work. I also want to thank Kerstin Janze and Yvonne Gabbey-Uebe for their administrative support as well as the technical staff of the institute, namely, Mr. Becker, Mr. Bieder, Mr. Egly, Mr. Ribbe and Mr. Rogge.

I kindly thank Priv. Doz. Dr. Armin Feldhoff for his support in SEM as well as Dr. Roland Marschall for helpful discussions and suggestions during my thesis.

Finally, I am especially grateful to my family Omolbanin Sharifi and Mohamad Bashir Sharifi, my brothers Zamir, Zubeir and Abas, my sister-in-law Nadera and my partner in life Sadaf for their continuous support during my entire thesis. Without these people none of this would have been possible.

Abstract

The presented thesis contains six original research articles dedicated to the preparation and characterization of organic-inorganic mesoporous materials as additives for polymer electrolyte membrane fuel cells (PEMFCs). The mesoporous materials Si-MCM-41 and benzene-PMO (periodic mesoporous organosilica) were chosen for the investigations. These materials were modified with functional groups for enhanced proton conductivity and water-keeping properties.

In order to improve these materials Brønstedt acidic groups were introduced in the framework of mesoporous Si-MCM-41. Therefore, some silicium atoms in the framework were substituted by aluminium using different aluminium sources. Here NaAlO_2 exhibits clearly the best results because the entire aluminium incorporated within the framework is tetragonally coordinated as observed by ^{27}Al MAS NMR. The increase of the proton conductivities results from an improved hydrophilicity, a decreased particle size, and newly introduced Brønstedt acidity in the mesoporous Al-MCM-41. However, mesoporous Si-MCM-41 materials functionalised by co-condensation with sulphonic acid groups exhibit the best results concerning proton conductivity, compared to those prepared by grafting. Hence, these materials were characterized in more detail by SANS and by MAS NMR measurements. The first one indicated that by co-condensation the entire inner pore surface is altered by functional groups which are, thus, distributed much more homogeneously than samples functionalised by grafting. This result explains the improved proton conductivities. Additionally, ^{29}Si NMR spectra proved that samples prepared by co-condensation lead to a successful and almost complete incorporation of mercaptopropyltrimethoxysilan (MPMS) into the mesoporous framework. Furthermore, it was shown by ^{13}C MAS NMR spectroscopy that the majority of the organic functional groups remained intact after H_2O_2 -oxidation. However, proton conductivity was further improved by using a more appropriate organic compound, namely bis(3-triethoxysilylpropyl)-disulfide (TESPD), and Br_2 as an optimum oxidising agent for a maximum yield of SO_3H -groups (98 %).

PMO materials of the type $(\text{R}'\text{O})_3\text{Si-R-Si}(\text{OR}')_3$ with benzene as organic bridge and a crystal-like periodicity within the pore walls were synthesised as alternative starting materials. The benzene-PMO materials offer a multiplicity of reactions due to the presence of organic bridges. In addition to that, the *crystalline* pore walls, proven by SANS during in-situ nitrogen adsorption measurements, open up new possibilities to form a regular distribution of anchored sulphonic acid groups. If the SO_3H -functionalisation of benzene-PMO materials was performed at both, benzene groups and silanol groups, a homogenous distribution of functional groups was achieved. Hence, a drastic increase of proton conductivity compared to pristine benzene-PMO and benzene-PMO with sulphonic acid grafted via propyl chains only on silica positions is observed.

Keywords: PEMFC membrane additives, solid proton conductors, functionalised mesoporous silica, PMO, SANS

Zusammenfassung

Die vorliegende Dissertation behandelt, in sechs ausgewählten Forschungsarbeiten, die Präparation und Charakterisierung von organisch-anorganischen mesoporösen Materialien als Additive für Polymerelektrolytbrennstoffzellen. Die mesoporösen Materialien Si-MCM-41 und Benzen-PMO wurden für die Untersuchungen ausgewählt. Diese Materialien wurden mit funktionellen Gruppen modifiziert, um ihre Leistung hinsichtlich Protonenleitfähigkeit und Wasserrückhalt zu verbessern.

Um die Eigenschaften des silicatischen Wirtsmaterials vor der Funktionalisierung zu optimieren, wurde am Beispiel von Si-MCM-41 Aluminium in das Gerüst eingebaut. Hierbei wurden einige Silizium Atome im mesoporösen Gerüst durch Aluminium ersetzt. Die Verwendung von NaAlO_2 als Al-Quelle erzielte die besten Ergebnisse in der Protonenleitfähigkeit, da das Aluminium tetragonal koordiniert im Gerüst vorliegt. Im Vergleich zur Grafting Methode, zeigten Si-MCM-41 Materialien, die mittels Co-Kondensation funktionalisiert worden waren, stets höhere Protonenleitfähigkeiten. Aus diesem Grund wurden diese Materialien über Kleinwinkel-Neutronenstreuexperimente und MAS NMR Messungen detaillierter charakterisiert. Für SO_3H -funktionalisiertes Si-MCM-41 konnte auf diesem Wege gezeigt werden, dass die Verteilung der Sulfonsäuregruppen nach einer Synthese mittels Co-Kondensation deutlich homogener ist als nach Grafting, und damit die höhere Protonenleitfähigkeit der durch Co-Kondensation erhaltenen Proben begründet. Außerdem bestätigten ^{29}Si NMR Spektren einen erfolgreichen und nahezu kompletten Einbau von Mercaptopropyltrimethoxysilan (MPMS). ^{13}C MAS NMR Auswertungen zeigten zudem, dass die funktionellen Gruppen auch nach der H_2O_2 -Oxidation intakt bleiben.

Um die Protonenleitfähigkeit weiter zu erhöhen wurde die organische Verbindung Bis(3-triethoxysilylpropyl)-disulfid (TESPD) verwendet. Zusätzlich wurde Br_2 als Oxidationsmittel eingesetzt, wodurch eine maximale Ausbeute an SO_3H -Gruppen erzielt werden konnte (98%).

Als alternative Ausgangsmaterialien wurden PMOs des Typs $(\text{R}'\text{O})_3\text{Si-R-Si}(\text{OR}')_3$ mit Benzen als organische Gruppe und einer quasi-kristallinen Periodizität innerhalb der Porenwand synthetisiert. Benzen-PMOs ermöglichen aufgrund ihrer organischen Gruppen eine Vielzahl von Funktionalisierungsmöglichkeiten. Die *Kristallinität* der Porenwände wurde mittels SANS Experimente und in-situ Stickstoffadsorption nachgewiesen und ermöglicht eine regelmäßige Verteilung von funktionellen Gruppen. Durch eine SO_3H -Funktionalisierung an den Benzengruppen als auch an den Silanolgruppen, wurde eine homogene Verteilung protonenleitender Gruppen erzielt. Die gemessenen Protonenleitfähigkeiten übertrafen deutlich die des reinen Benzen-PMOs.

Stichwörter: PEMFC Additive, protonenleitende Festkörper, funktionalisierte mesoporöse Silica, PMO, SANS

Contents

1	INTRODUCTION.....	1
1.1	Motivation	1
1.2	Fuel Cell Technology	3
1.2.1	Proton Exchange Membrane Fuel Cell.....	7
1.3	Proton Conductivity Mechanisms	8
1.4	Inorganic-Organic Composite Membranes.....	10
1.5	Mesoporous Materials	12
1.5.1	Introduction of Mesoporous Materials	12
1.5.2	MCM-41	14
1.5.3	Functionalisation Methods for Mesoporous Materials	15
1.5.4	Periodic Mesoporous Organosilicas	17
2	PROTON CONDUCTIVITY OF ALUMINIUM FUNCTIONALISED SI-MCM-41	19
2.1	Summary	19
2.2	Proton Conductivity of Ordered Mesoporous Materials Containing Aluminium.....	20
3	CHARACTERIZATION OF SI-MCM-41-SO₃H BY SANS AND MAS NMR.....	21
3.1	Summary	21
3.2	Detection of Homogeneous Distribution of Functional Groups in Mesoporous Silica by Small Angle Neutron Scattering and in-situ Adsorption of Nitrogen or Water.....	22
3.3	Detection Proton Conducting Sulphonic Acid Functionalized Mesoporous Materials Studied by IS, MAS NMR Spectroscopy and MAS PFG NMR Diffusometry	23
4	INVESTIGATION ON PROTON CONDUCTING SO₃H-FUNCTIONALISED BENZENE-PMO.....	24
4.1	Summary	24
4.2	Proton conductivity of SO ₃ H-functionalised benzene-PMO	25
4.3	Small Angle Neutron Scattering and in-situ Adsorption of Nitrogen Study on Periodic Mesoporous Organosilica Materials.....	26
5	ENHANCED PROTON CONDUCTIVITY BY MORE APPROPRIATE FUNCTIONAL GROUPS AND OXIDATION METHODS.....	39
5.1	Summary	39
5.2	Investigation on the Optimal Oxidation Agent for a Maximum Yield of Sulphonic Acid Groups in MCM-41	40
6	CLOSING REMARKS.....	41
7	APPENDIX.....	44

1 Introduction

1.1 Motivation

Although various media report about falling birth rates, the United Nations estimate that the world population will increase from 7 billion to 9.2 billion by the year 2050.^{1,2} At the same time, the desire for mobility and comfort, and thus the demand for energy, increases.^{3,4} However, the growing world population and rising energy requirements are in contradiction to the amount of available fossil fuels. In addition, wasteful consumption and the recovery of these non-renewable fossil fuels have a strong environmental impact, since substances in the atmosphere, such as nitric oxides and carbon dioxide, are decomposing the ozone layer.⁵ As a consequence of this the protection ability of the ozone layer against ultraviolet radiation is decreased, which is potentially damaging to all life forms on earth, especially for phytoplanktons, which produce more than 50 % of the oxygen in the atmosphere during photosynthesis. Hence, the natural greenhouse effect is greatly intensified, causing global warming.⁶ In the long term, this would have fatal consequences for mankind. Therefore, alternative energy sources are in the focus of recent research. Two promising technologies, usually stationarily used to transform natural energy into electrical energy, are solar⁷ and wind energy,⁸ respectively. Another environmentally friendly production of energy is made possible by fuel cell technology - which is used for mobile applications.^{9,10} This converts chemical energy directly into electrical energy by the reaction of hydrogen and oxygen into water. The most used methods for hydrogen production are reforming¹¹ and water electrolysis.¹² It is thus a secondary energy, since primary energy is always expended for its production. A completely environmentally friendly energy production by hydrogen takes place only if renewable energy sources are used for its production. The fuel cell consists of two electrodes that are located in electrolyte solutions, which are separated by a proton-conducting membrane. The electrodes are connected

¹ G. Dubois, P. Peeters, J.P. Ceron, and S. Gössling, *Transportation Research* **2011** (45), 1031-1042.

² A.B. Stambouli and E. Traversa, *Renewable and Sustainable Energy Reviews* **2002**, (6), 297-3036.

³ K. Mori, *Journal of the Japan Institute of Energy* **2004** (82), 594-602.

⁴ International Energy Agency. World Energy Outlook 2008, Fact Sheet, IEA/AIE, Paris 2008.

⁵ F.S. Rowland, *Philosophical Transactions of the Royal Society B: Biological Sciences* **2006** (361), 769-790.

⁶ C. Parmesan and G. Yohe, *Nature* **2003** (421), 37-42.

⁷ U. Bach, D. Lupo, P. Comte, J.E. Moser, F. Weissörtel, J. Salbeck, H. Spreitzer, and M. Grätzel, *Nature* **1998** (395), 583-585.

⁸ M.I. Hoffert, K. Caldeira, G. Benford, D.R. Criswell, C. Green, H. Herzog, A.K. Jain, and T.M.L. Wigley, *Science* **2002** (298), 981-987.

⁹ C.K. Dyer, *Journal of Power Sources* **2002** (106), 31-34.

¹⁰ J.A. Paradiso and T. Starner, *IEEE Pervasive Computing* **2005** (4), 18-27.

¹¹ R.D. Cortright, R.R. Davda, and J.A. Dumesic, *Nature* **2002** (418), 964-967.

¹² H. Iwahara, T. Esaka, H. Uchida, and N. Maeda, *Solid State Ionics* **1981** (3), 359-363.

via an external circuit with a consumer and are bathed in reactant gases. A major type of fuel cell is the PEMFC. The most important, high efficient, and life insuring component of a PEMFC is the proton-conducting membrane. These membranes must satisfy two relevant requirements: 1) allow proton transport from the anode to the cathode, and 2) act as a gas separating barrier (H_2 , O_2). In general, they are made of organic polymers containing acidic functionalities such as carboxylic, sulphonic or phosphoric groups.^{13,14} In the presence of water, dissociation takes place, allowing H_3O^+ -hydrated proton transport. Hence, the performance of the membrane depends on the amount of ionic groups and on the hydration rate. Its development is therefore in the focus of current research, in order to improve PEMFCs.^{15,16} Currently, Nafion[®] is the most often used polymer membrane in PEMFCs,¹⁷ combining a hydrophobic perfluorinated backbone with hydrophilic side chains carrying very strong acidic end groups ($-SO_3H$). The SO_3H -groups are necessary for the proton conductivity, as well as for the interaction with hydrophilic water molecules. A major drawback of Nafion[®] nonetheless continues to be the difficulty to maintain a defined high relative humidity, which is necessary to avoid swelling or shrinking of the membrane and the complete loss of proton conductivity at temperatures above 373 K when water is evaporating. Hence, the highest application temperature for Nafion[®] is 353 K.¹⁸ Higher working temperatures of about 413-453 K, however, are favourable, as the cooling of the fuel cell is simplified (in mobile systems), the tolerance towards carbon monoxide, which poisons the expensive platinum electro catalyst, is increased, and finally, the faster cathode kinetics lead to smaller amounts of the noble metal catalyst. For this reason, there is a great interest in developing alternative membranes for fuel cells, which show high proton conductivity, high temperature water-keeping properties, and are made of low-cost thermo stable polymers. Possible candidates are aromatic-based polymers, such as polysulphones (PPSU),¹⁹ poly (benzimidazoles) (PBI),²⁰ poly(-imides), or the so called poly(aryletherketones) PEEK.²¹ These materials, however, need to be functionalised with proton conducting sulphonic acid groups.

A promising approach for future generations of membranes for PEMFC is the incorporation of solid inorganic-organic additives to the polymer membrane, such as: TiO_2 , SiO_2 , SnO_2 , ZrO_2 , or certain zeolites.²² The preparation of these membranes is

¹³ Q. Li, R. He, J.O. Jensen, and N.J. Bjerrum, *Chemistry of Materials* **2003** (15), 4896-4915.

¹⁴ C. Song, *Catalysis Today* **2002** (77), 17-49.

¹⁵ J.W. Fergus, *Journal of Power Sources* **2006** (162), 30-40.

¹⁶ Z.G. Shao, P. Joghee, and I.M. Hsing, *Journal of Membrane Science* **2004** (229), 43-51.

¹⁷ B. Ladewig, *Nafion Nanocomposite Membranes for the DMFC*, Vdm Verlag Dr. Müller, 2008.

¹⁸ K.A. Mauritz and R.B. Moore, *Chemical Reviews* **2004** (104), 4535-4585.

¹⁹ J. Kerres, W. Cui, and S. Reichle, *Journal of Polymer Science* **1996** (34), 2421-2427.

²⁰ Y.L. Ma, J.S. Wainright, M.H. Litt, and R.F. Savinell, *Journal of the Electrochemical Society* **2004** (151), 8-16.

²¹ D.J. Jones and J. Roziere, *Journal of Membrane Science* **2001** (185), 41-48.

²² C. Laberty-Robert, K. Valle, F. Pereira, and C. Sanchez, *Chemical Society Reviews* **2011** (40), 961-1005.

implemented by dip-coating,²³ casting,²⁴ spraying,²⁵ or spin coating.²⁶ It is, however, very difficult to obtain homogenous membranes due to particle agglomeration and segregation inside the polymer matrix, especially for micro-sized particles.²⁷ Nevertheless, several authors have illustrated an improved performance of the membrane at high temperatures and low humidity for different organic-inorganic composite membranes with highly dispersed metal oxide particles in the structure of Nafion®.^{28,29} Another approach to prepare new organic-inorganic composite membranes is to synthesise ordered mesoporous solids functionalised with proton conducting groups. Compared to non-porous and non-ordered materials, they show many advantages, including: (i) a higher amount of proton conducting groups due to high surface area, (ii) the absorption of water inside the pore volume and hence increased water-keeping properties, as well as (iii) their long-range ordered mesopores, which can help to guide protons through their pore channels.

1.2 Fuel Cell Technology

The idea to produce electricity with the help of the fuel cell is more than 170 years old. In 1838 Prof. F. Schönbein (1799-1868) found that a current is generated by the reversible reaction of hydrogen and oxygen gas. Based on these results, William Grove developed the first fuel cell ("galvanic gas battery") in the same year.³⁰ Here, two platinum electrodes were immersed in sulphonic acid and flushed with hydrogen or oxygen. In order to increase the activity of the platinum electrodes, a deposited layer of Pt-sponge was used in each glass tube. However, after 1866 Werner von Siemens developed the first dynamo and the interest in fuel cells vanished, due to the electro-dynamic principle providing much easier electrical power and the knowledge in the field of electrochemistry being sufficient. In the middle of the 20th century the National Aeronautics and Space Administration (NASA) used an alkaline fuel cell (AFC) successfully for the first time in the aerospace industry.³¹ Since high investment costs made further processing very difficult, though, fuel cells continued to be used only in aerospace and the military sector. At the end of the nineties, the

²³ H. Choi, E. Stathatos, and D.D. Dionysiou, *Applied Catalysis B: Environmental* **2006** (63), 60-67.

²⁴ C. Genies, R. Mercier, B. Sillion, N. Cornet, G. Gebel, and M. Pineri, *Polymer* **2001** (42), 359-373.

²⁵ C. Sanchez, C. Boissiere, D. Grosso, C. Laberty, and L. Nicole, *Chemistry of Materials* **2008** (20), 682-691.

²⁶ C.J. Brinker, Y. Lu, A. Sellinger, and H. Fan, *Advanced Materials* **1999** (11), 579-586.

²⁷ M. Uchida, Y. Aoyama, N. Eda, and A. Ohta, *Journal of the Electrochemical Society* **1995** (142), 463-468.

²⁸ A.K. Sahu, G. Selvarani, S. Pitchumani, P. Sridhar, and A. K. Shukla, *Journal of Electrochemistry Society* **2007** (154), 123-128.

²⁹ A. Sacca, A. Carbone, E. Passalacqua, A.D. Epifonia, S. Licocchia, E. Traversa, E. Sala, F. Traini, and R. Ornelas, *Journal of Power Sources* **2005** (152), 16-23.

³⁰ www.diebrennstoffzelle.de, December 2011.

³¹ B.Y.S. Lin, D.W. Kirk, and S.J. Thorpe, *Journal of Power Sources* **2006** (161), 474-483.

interest in fuel cell technology increased, especially by the automotive industry due to the scarcity of current energy resources.³²

Every fuel cell is composed of two electrodes, a cathode and an anode. Hydrogen and oxygen react in a controlled platinum catalysed reaction to form water ("cold combustion"). At the anode, hydrogen molecules are oxidised to form hydrogen cations and electrons, which pass through an electrical conductor (bipolar plate) to the cathode, where oxygen atoms are reduced. Conventional fuel cell systems with Nafion[®] proton conducting membranes operate at around 348 K and an operating pressure between 2.5 and 18 bar, depending on the fuel cell system used and its application. The excess pressure ensures the wetting of the membrane.

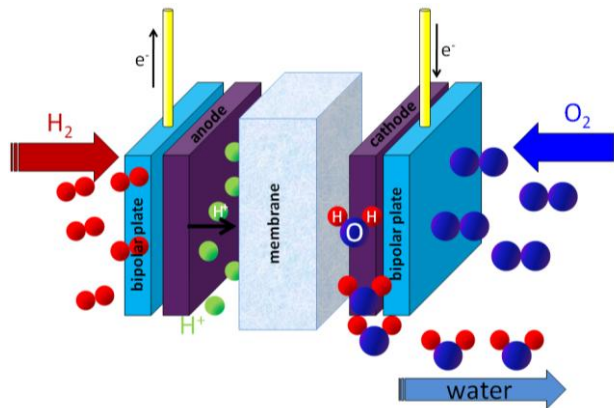
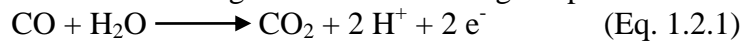
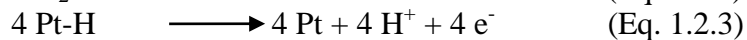


Figure 1: Fuel cell assembly.

The formation of harmless carbon dioxide is illustrated in Equation 1.2.1, which, compared to carbon monoxide, does not block absorption sites on the platinum catalyst surface. The yield of carbon dioxide grows with increasing temperature.



The platinum catalyst is needed due to the high activation energy of hydrogen and oxygen dissociation. During the first reaction step, the formation of an intermediate hybrid compound takes place, followed by the dissociation of this platinum hydride and the formation of protons and electrons.



At the anode side, the recombination of protons, electrons, and oxygen takes place.

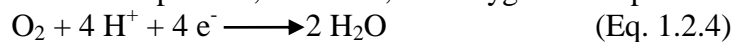


Figure 2 shows the most important fuel cell types. They all have in common that hydrogen reacts with oxygen, yet differ in their implementation, since they employ different electrolytes and temperatures.

³² A.E. Farrell, R.J. Plevin, B.T. Turner, A.D. Jones, M. O'Hare, and D.M. Kammen, *Science* **2006** (311), 506-508.

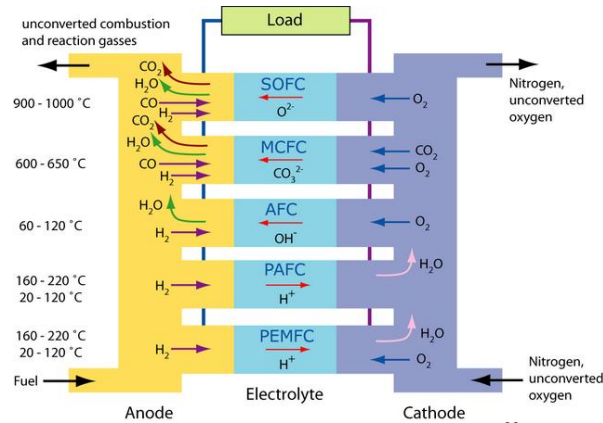


Figure 2: Different types of fuel cells.³³

One of the most important properties rendering the fuel cell technology as very attractive is its thermodynamic efficiency. For instance, the theoretical maximum efficiency of an ideal hydrogen-oxygen fuel cell is 94.5 %.³⁴ However, depending on the operating temperature and the type of fuel cell efficiencies in practice, the efficiency is minimised to about 40 %. This is explained by the fact that the output voltage (U) is always lower than the theoretical voltage called “open circuit voltage” (U_{th}). These losses depend on the current density and are determined by the kinetics of electrode reactions. The resulting voltage (U) is determined by the following equation:

$$U = U_{th} - \Delta U \quad (\text{Eq. 1.2.5})$$

ΔU is the sum of all voltage losses, which are shown in Figure 3. ΔU_{rev} is the reversible voltage loss. ΔU_A is the voltage loss which is caused by cathode and anode polarizations, as well as by the activation process for electrochemical reactions. A nearly linear fall in voltage can be observed as the current density increases, since there is a resistance to current flow within the fuel cell according to Ohm’s Law. At very high current densities, the hydrogen reaction rate is also high. The hydrogen cannot diffuse to the electrode fast enough to react, however, limiting mass transfer and causing rapid voltage drops to zero (ΔU_{diff}).

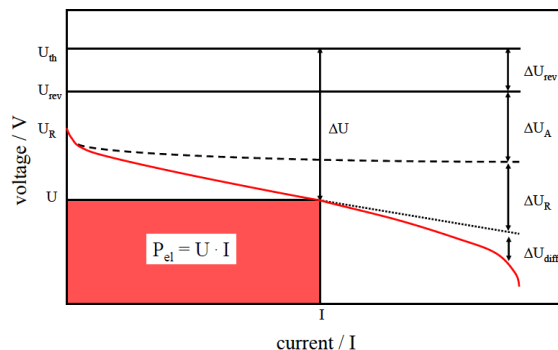


Figure 3: Voltage losses in fuel cell operation due to electrode kinetics.³⁵

³³ www.brennstoffzelle-nrw.de/index.php?id=39 (11/2011).

³⁴ F. Barbir and T. Gómez, *International Journal of Hydrogen Energy* **1996** (21), 891-901.

³⁵ Dissertation R. Marschall, *New solid proton conductors: Functionalized mesoporous SiO₂ materials for application in high temperature PEM fuel cell membranes*, Hannover, p.19.

A comparison between a fuel cell and a Carnot heat engine is illustrated in Figure 4. While in the case of a Carnot heat engine electrical energy derives only with detours from chemical energy, fuel cells directly produce electrical energy.³⁶ In addition, fuel cells have a much greater efficiency, since it is not limited by the Carnot factor.

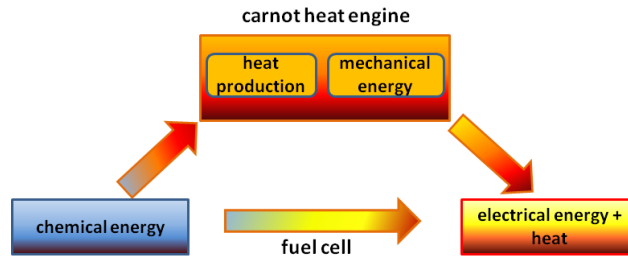


Figure 4: Energy conversions in a Carnot or fuel cell process.

In Figure 5, Carnot efficiency is compared with the theoretical efficiency of a H₂/O₂ fuel cell's function contingent upon temperature. While the efficiency of a Carnot heat engine increases with increasing temperature, it decreases in the case of a fuel cell. This can be explained by the calculation of efficiencies.

Carnot Heat Engine

$$\eta_{el} = \frac{T_2 - T_1}{T_2} = 1 - \frac{T_1}{T_2} \quad | \quad T_2 > T_1 \quad (\text{Eq. 1.2.6})$$

T₁: outlet temperature

T₂: operation temperature

The Equation (1.2.6) shows that increasing operation temperature (T₂) leads to an increase in the efficiency of a heat-power engine. In contrast, the efficiency of a fuel cell is calculated from the free reaction enthalpy, standard reaction entropy, and the standard formation enthalpy.

H₂/O₂-Fuel Cell

$$\eta_{el} = \frac{\Delta_R G^\circ}{\Delta_f H^\circ} = \frac{\Delta_f H^\circ - T_2 \cdot \Delta_R S^\circ}{\Delta_f H^\circ} = 1 - \frac{T_2 \cdot \Delta_R S^\circ}{\Delta_f H^\circ} \quad (\text{Eq. 1.2.7})$$

Δ_fH°: standard formation enthalpy

Δ_RG°: free reaction enthalpy

Δ_RS°: standard reaction entropy

Here, two different values are possible (depending on the operation temperature) for the standard enthalpy Δ_fH°:

i) combustion of hydrogen:



³⁶ M.W. Ellis, M.R. Von Spakovsky, and D.J. Nelson, *Proceedings of the IEEE* **2001** (89), 1808-1817.

ii) condensation to liquid water:



In order to obtain higher values for the efficiencies, the LHV is used almost exclusively in literature.^{37,38} Equation (1.2.7) shows that, in contrast to a Carnot heat engine, an increase in temperature causes a decrease in efficiency.

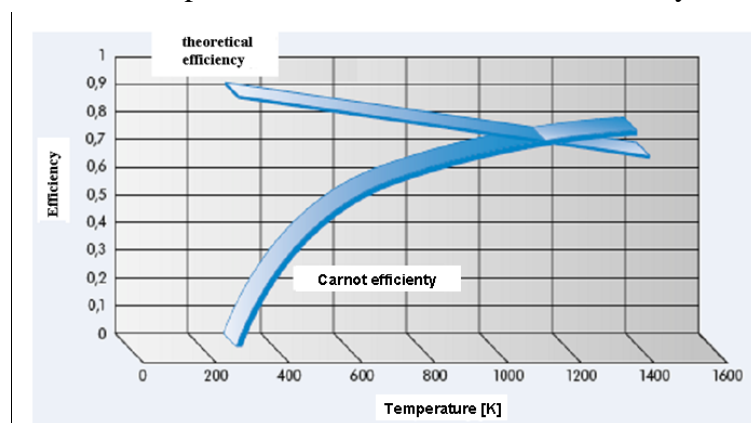


Figure 5: Ideal efficiency of a hydrogen-oxygen fuel cell against the Carnot efficiency depending on the temperature T_2 .²⁹

1.2.1 Proton Exchange Membrane Fuel Cell

The focus of this thesis lies on additives for proton conducting polymer membranes used in PEMFC (Fig. 6). Therefore, a more detailed description of this type of fuel cell follows.

Compared to other types of fuel cells, PEMFCs exhibit some advantages. They generate a high power density,³⁹ start up quickly,⁴⁰ owing to the electrolyte working at low temperatures, and are also tolerant to shock and vibration due to plastic materials and an immobilised electrolyte.⁴¹ The latter also simplifies the sealing of the anode and the cathode with respect to diffusion of gases. The heart of the fuel cell is the proton conducting membrane and must fulfil several requirements:

- high ionic conductivity for rapid transport of the respective ionic species,
- low permeability of the reactants (gas and fuel),
- electrically non-conductive to prevent electrical short circuit,
- chemical and mechanical long-term resistance,
- good water uptake, and
- thermal stability.

³⁷ S.H. Chan, C.F. Low, and O.L. Ding, *Journal of Power Sources* **2002** (103), 188-200.

³⁸ S. Miachon and P. Aldebert, *Journal of Power Sources* **1995** (56), 31-36.

³⁹ C. Lim and C.Y. Wang, *Electrochimica Acta* **2004** (49), 4149-4156.

⁴⁰ J.H. Kim, E.A. Cho, J.H. Jang, H.J. Kim, T.H. Lim, I.H. Oh, J.J. Ko, and I.J. Son, *Journal of the Electrochemical Society* **2010** (157), 118-124.

⁴¹ W. Glasspool and J. Atkinson, *Sensors and Actuators* **1998** (1-3), 308-317.

There are several polymer membrane systems which are competitive for use in PEMFC systems: perfluorinated polymers with proton-conducting sulphonic acid groups like Nafion[®] (Dupont de Nemours),⁴² Dow[®] (Dow Chemical),⁴³ Flemion[®] (Asahi Chemical),⁴⁴ or Aciplex-Ss (Asahi Glas).⁴⁵ However, all these materials are limited to low operation temperature and/or high humidity. Beside the two electro catalytic electrodes, which are separated by the proton conducting membrane, bipolar plates are used around the membrane electrode assembly (MEA) (Fig. 6). These regulate the flow of reactant gases and the removal of product water. In addition, they are also responsible for heat evacuation and electrical contact. Since the voltage of a single PEMFC (1.23 V at 298 K) is not sufficient, several cells are assembled into a fuel cell stack.⁴⁶

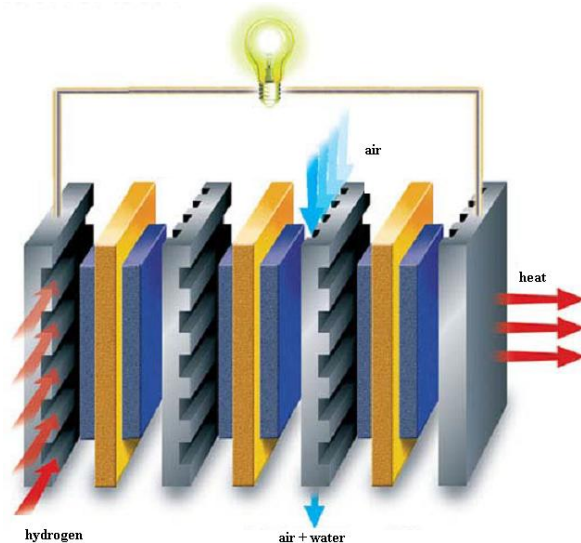


Figure 6: PEMFC stack with construction elements.⁴⁷

1.3 Proton Conductivity Mechanisms

In general, three mechanisms are used to describe proton conductivity in the case of the polymer electrolyte membranes:

- I. surface diffusion along functional groups,
- II. structural diffusion according to the Grotthuss mechanism, and
- III. the vehicle mechanism, diffusion of mobile species.

Gierke et al. presented an example for surface diffusion which uses the cluster-network model for Nafion[®].⁴⁸ Thus, there is a classic transfer of protons along the

⁴² S.C. Yeo and A. Eisenberg, *Journal of Applied Polymer Science* **1997** (21), 875-898.

⁴³ M. Wakizoe, O.A. Velev, and S. Srinivasan, *Electrochimica Acta* **1995** (40), 335-343.

⁴⁴ N. Yoshida, T. Ishisaki, A. Watakabe, and M. Yoshitake, *Electrochimica Acta* **1998** (42), 3749-3757.

⁴⁵ www.hydrogen.energy.gov/program_plans.html, December 2011.

⁴⁶ J. Hamelin, K. Agbossou, A. Laperrière, F. Laurencelle, and T.K. Bose, *International Journal of Hydrogen Energy* **2001** (26), 625-629.

⁴⁷ www.fctec.com, December 2011.

functional sulphonic acid anions which protrude into the non-ordered clusters that were formed by the swelling of the Nafion[®] membrane and exhibit different pore diameters. This mechanism is superimposed in highly hydrated proton conductors, such as Nafion[®], by the Grotthuss mechanism.⁴⁹ In this case, the water molecules in Nafion[®] form via hydrogen bonds molecular chains in which the proton is transferred by structural defects, thus, by hydrogen bond breaking and formation.

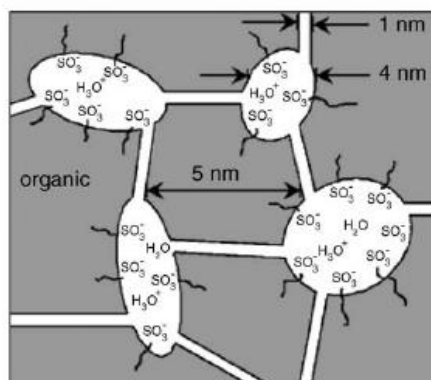


Figure 7: Cluster-network model.⁴⁸

Hereby, two intermediate ions are formed: the Zündel ion (H_5O_2^+) and the Eigen ion (H_9O_4^+), which enable proton transport. The transfer time of a proton from a Zündel ion to an Eigen ion lies in the range of 1.3-1.5 ps, followed by the transformation of the Eigen ion back to the Zündel ion, as shown in Figure 8.

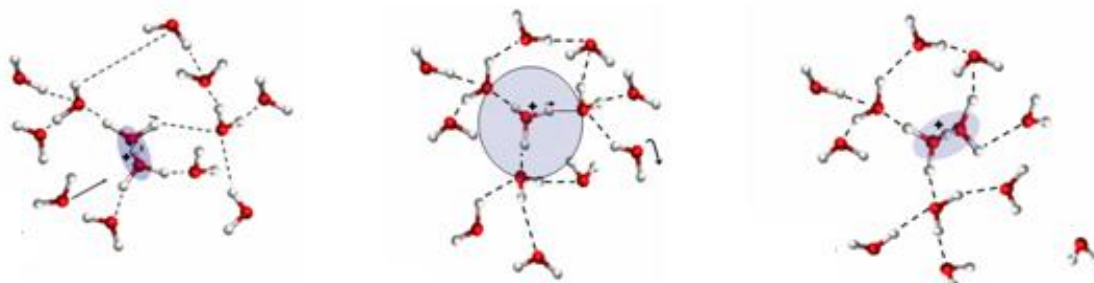


Figure 8: Proton transfer from Zündel-ion (left) over Eigen-ion (middle) to Zündel-ion (right).

The Zündel-ion exhibits a hydroxonium-ion (H_5O_2^+) in the centre of the water cluster, which is coordinated four times by water molecules (Fig. 8, left). The proton which is placed between two oxygen atoms hops to one of them, leading to a charged atom with three hydrogen bonds. This hydronium-ion (H_3O^+) is solvated by three water molecules via hydrogen bonds and forms the Eigen-ion (Fig. 8, middle).

The vehicle mechanism is based on the attachment of a proton to a water molecule, leading to the formation of a vehicle (H_3O^+) or a larger complex (H_5O_2^+ or H_9O_4^+). The formation of protons by the oxidation of hydrogen at the anode leads to a high proton concentration. The resulting concentration gradient causes a diffusion of the formed vehicle through the membrane towards the cathode and thus the transport of

⁴⁸ W.Y. Hsu and T.D. Gierke, *Journal of Membrane Science* **1983** (13), 307-326.

⁴⁹ N. Agmon, *Chemical Physics Letters* **1995** (244), 456-462.

protons from anode to cathode. In contrast to the Grotthuss mechanism, no hydrogen bond breaking and formation causes the proton transport. Hence, the proton transport depends on the diffusion coefficient of the vehicle.

1.4 Inorganic-Organic Composite Membranes

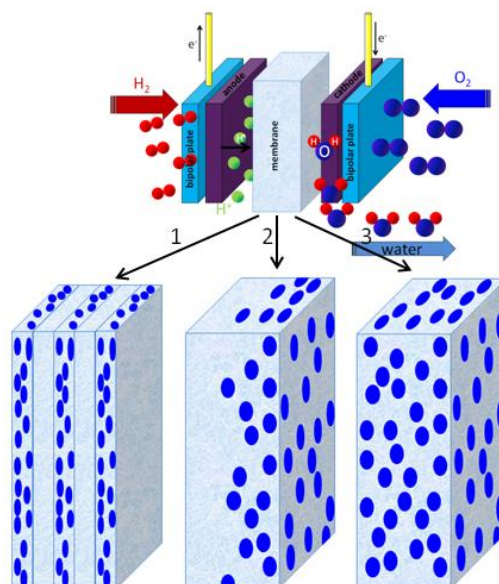


Figure 9: Different types of composite inorganic-organic membranes.

The focus of this work is not the development of new proton-conducting polymers, but the improvement of water storage of current Nafion[®]-based systems by suitable organic/inorganic proton-conducting additives.

There are already numerous studies that show that homogeneous distribution of inorganic particles improves the performance of a Nafion[®] membrane at high temperature and low humidity.⁵⁰ Sahu et al. investigated Nafion[®]-silica-membranes with different amounts of SiO₂ (2.5-15 wt-%).²⁸ The composite membranes showed improved performance in a wide range of humidity, compared to pure Nafion[®], which is explained by the increased water affinity due to the SiO₂ particles supporting the proton conductivity at low humidity and high temperature. Possible proton conducting groups in the membrane or on the surface of the additives may be imidazole,⁵¹ phosphoric acid,⁵² or sulphonic acid groups.⁵³ The latter have proved to be more advantageous for the use in PEMFC systems.⁵⁴ A promising alternative to the previously used, most non-porous or microporous nanoparticle additives for

⁵⁰ A. Sacca, A. Carbone, E. Passalacqua, A. D. Epifonia, S. Licocchia, E. Traversa, E. Sala, F. Traini, and R. Ornelas, *Journal of Power Sources*, **2005** (115), 16-24.

⁵¹ R. Marschall, M. Sharifi, and M. Wark, *Microporous and Mesoporous Materials* **2009** (123), 21-29.

⁵² R. He, Q. Li, G. Xiao, and N.J. Bjerrum, *Journal of Membrane Science* **2003** (226), 169-184.

⁵³ R. Marschall, I. Bannat, J. Caro, and M. Wark, *Microporous and Mesoporous Materials* **2007** (99), 190-196.

⁵⁴ M. Schuster, T. Rager, A. Noda, K. D. Kreuer, and J. Maier, *Fuel Cells* **2005** (5), 355-362.

proton-conducting membranes, are ordered mesoporous solids.⁵⁵ Li et al. reported sol-gel-derived mesostructured zirconium phosphates with proton conductivities of about $1 \cdot 10^{-6}$ - $1 \cdot 10^{-8}$ S/cm.⁵⁶ Although the conductivity values of these mesoporous acid free silica xerogels or anatase thin films show good proton conductivity, their performance as an electrolyte in a PEMFC has not yet been tested.²⁵ Compared to these nonfunctionalised materials, organic acid modified materials prepared by grafting or by co-condensation, have shown better proton conductivities.⁵⁷ For example, acid functionalised zeolite nanocrystals showed proton conductivities in the range of $1.2 \cdot 10^{-3}$ - $2 \cdot 10^{-2}$ S/cm,⁵⁸ which are one or two orders of magnitude lower than those of Nafion[®] at 100 % relative humidity and room temperature. The proton conductivity depends on the degree of functional groups, acid strength, and the pore structure. McKeen et al. have studied proton conductivity of a series of pure-silica zeolite beta, MCM-41, and MCM-48 containing sulphonic acids, phosphoric acid, or carboxylic acid groups.⁵⁹ They found that aryl sulphonic acid functionalised samples showed the highest proton conductivity, followed by materials functionalised with propyl sulphonic acid, phosphoric acid, and carboxylic acid. Furthermore, mesoporous materials showed higher proton conductivities compared to the microporous materials, MCM-41 materials are also more conductive than the corresponding MCM-48.

Thus, compared to materials with non-ordered pore structure, organically functionalised silica materials with high pore ordering, such as SBA-15, MCM-48, and especially MCM-41, are promising additives for fuel cell applications. An alternative way to obtain inorganic-organic ordered porous materials is obtained by the synthesis of PMOs, where organic groups are already incorporated in a three-dimensional network structure (section 1.5.4). The hydrophilic nanoparticles can be used to derive the resulting product water at the cathode to humidify the membrane. Decisive factors are the nature, extent, and density of the functional groups, and the distribution of the mesoporous nanoparticles in the polymer matrix (Fig. 9, sandwich-structure (1), inhomogeneous distribution (2), and homogenous distribution (3)), so that the water and protons can perform optimally in their pore systems and the product water can be distributed homogeneously throughout the membrane. The performance of future generations of fuel cell membranes, which operate at temperatures above 373 K and low humidity, will significantly depend on the optimisation of these proton-conducting porous additives.

⁵⁵ M. Yamada, D. Li, I. Honma, and H. Zhou, *Journal of the American Chemical Society* **2055** (127), 13092-13093.

⁵⁶ H.B. Li and M. Nogami, *Advanced Materials* **2002** (14), 912-922.

⁵⁷ R. Marschall, I. Bannat, A. Feldhoff, L. Wang, G.Q. Lu, and M. Wark, *Small* **2009** (5), 854-865.

⁵⁸ C.A Alabi and M.E. Davis, *Chemistry of Materials* **2006**, (18), 5634-5642.

⁵⁹ J.C. McKeen, Y.S. Yan, and M.E. Davis, *Chemistry of Materials* **2008** (20), 5122-5124.

1.5 Mesoporous Materials

1.5.1 Introduction of Mesoporous Materials

Mesoporous materials are very important in nature and technology due to their physical and chemical properties.^{60,61} According to the International Union of Pure and Applied Chemistry (IUPAC), the porous materials are divided into three groups (Table 1).

Table 1: Nanoporous materials according to the IUPAC.

material	pore diameter	example
microporous	$D \leq 2$ nm	zeolite
mesoporous	$2 \text{ nm} < d \leq 50$ nm	MCM-41, SBA-15
macroporous	$D > 50$ nm	porous glass

The first materials with ordered mesoporous and uniform pore diameters were introduced in 1992 by the Mobil Oil Corporation (Mobil's Composition of Matter, MCM). Depending on which template is used, a pore diameter size of 1.5-10 nm is possible.⁶² Figure 10 shows three materials of the M41S family: MCM-50, MCM-41, and MCM-48.⁶³

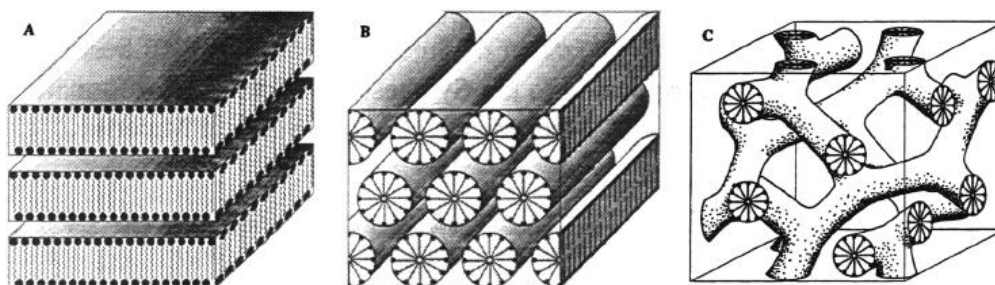


Figure 10: Description of three M41S phases: A) lamellar MCM-50, B) hexagonal MCM-41, C) cubic MCM-48.⁶³

For the synthesis of MS41S materials quaternary ammonium cations and anions such as bromides, chlorides, or hydroxides are used. These surfactants consist of a polar, hydrophilic head group, and a hydrophobic chain. The hydrophilic head group can be cationic,¹⁹ anionic,⁶⁴ zwitterionic,⁶⁵ or neutral.⁶⁶ Surfactants are surface active and thus reduce the surface tension of a solvent.

⁶⁰ M. Hartmann, *Chemistry of Materials* **2005** (17), 4577-4593.

⁶¹ Y. Tao, H. Kanoh, L. Abrams, and K. Kaneko, *Chemical Reviews* **2006** (106), 896-910.

⁶² C.T. Kresge, M.E. Leonowicz, W.J. Roth, J.C. Vartuli, and J.S. Beck, *Nature* **1992** (352), 84-87.

⁶³ Q. Huo, D.I. Margolese, and G.D. Stucky, *Chemistry of Materials* **1996** (8), 1147-1160.

⁶⁴ A. Badiei, R. Vahidifar, and A. Hasheminasab, *Iranian Journal of Chemistry* **2008** (12), 352-359.

⁶⁵ J.W. Park, D.S. Jung, and M.E. Seo, *Microporous and Mesoporous Materials* **2008** (112), 265-276.

⁶⁶ J. Demel, J. Cejka, and P. Stepnicka, *Journal of Molecular Catalysis* **2007** (112), 26-34.

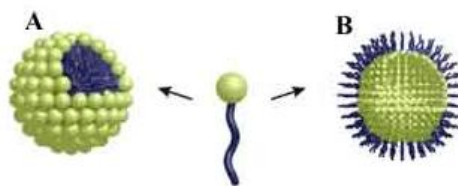


Figure 11: Micelle formation in different media: water (A) and oil (B).⁶⁷

At a certain concentration, the surfactant forms micelles (critical micelle concentration, cmc). Depending on which solvent is used, micelles of the type A (polar solvent) or type B (non-polar solvent) are obtained (Fig. 11). The formation of spherical micelles is preferred, since the ratio between volume and surface is minimal and thus yields a maximum value of entropy. The micelle structure depends on the concentration of the surfactant in water and on the temperature (Fig. 12). When the concentration of the surfactant is further increased, different types of aggregates can be obtained: rod-like, mesophase, or lamellar phase.⁶⁸

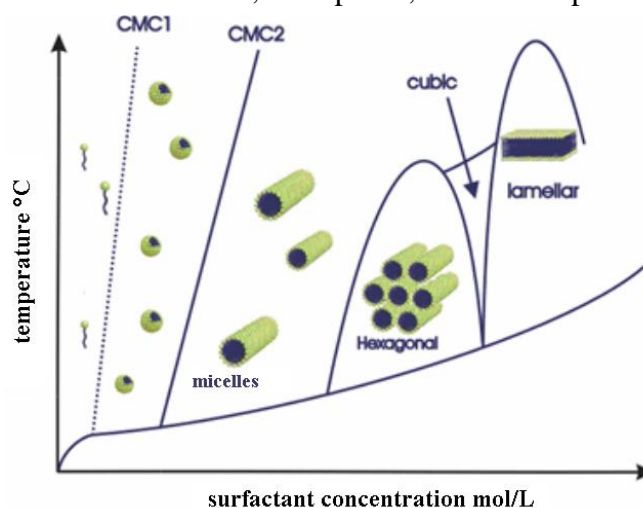


Figure 12: Phase diagram for the binary system Cetyltrimethylammoniumbromide (CTAB) in water, depending on surfactant concentration and temperature.

Table 2 gives an overview of the possible aggregates, the resulting structure, as well as an example for each structure. The package-parameter P can be calculated as follows:

$$P = \frac{V}{A_0 L_c} \quad (\text{Eq.1.5.1.1})$$

V : chain length

A_0 : surface of the head group

L_c : chain length

⁶⁷ J.A. Elemans, A.E. Rowan, and R.J.M. Nolte, *Journal of the American Chemical Society* **2002** (124), 263-266.

⁶⁸ C. Tanford, *Journal of Physical Chemistry* **1972** (76), 88-92.

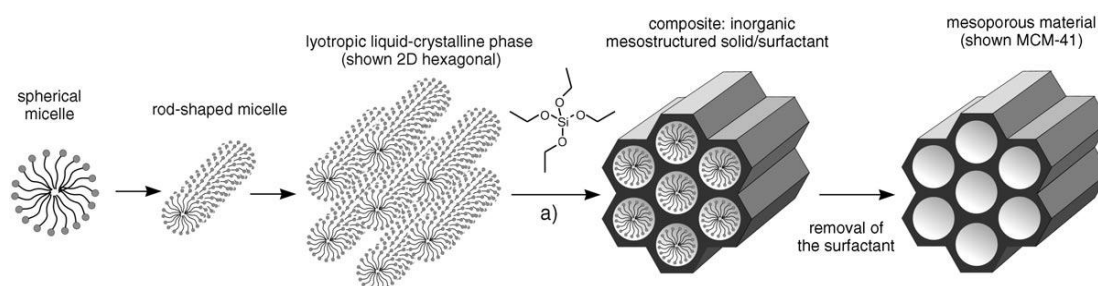
Table 2: Expected structure depending on the package-parameter P.

P	Structure	example
$\frac{1}{3}$	cubic	SBA-1
$\frac{1}{2}$	hexagonal	MCM-41, FSM-16, SBA-3
$\frac{1}{2}-\frac{2}{3}$	cubic	MCM-48
1	lamellar	MCM-50

1.5.2 MCM-41

MCM-41 is the most important compound of the M41S family and exhibits a regular hexagonal arrangement of cylindrical mesopores. For their synthesis, a silica source like sodium silicate or tetraethylorthosilicate (TEOS) is typically used.

The formation mechanisms for the M41S materials are shown in Figure 13 and 14. The synthesis of the desired mesoporous material can be achieved through two possible ways. One of the most accepted mechanisms, the true liquid template mechanism (TLCT), is shown in Figure 13. After the formation of rod-shaped micelles from amphiphilic molecules, an ordered hexagonal structure is built. The inorganic Si-molecules (here TEOS) are deposited subsequently to the micelles. However, $^1\text{H-NMR}$ and transmission electron microscopy (TEM) showed that the concentration of the surfactant was far below the cmc.⁶⁹ Thus, the formation of these mesostructures cannot be explained by the route in Figure 13.

Figure 13: Formation mechanisms of MCM-41.⁷⁰

Another explanation is shown in Figure 14, the so called cooperative self-organisation process mechanism, which was proposed by Firouzi et al. based on $^1\text{H-NMR}$, $^{29}\text{Si-NMR}$, and neutron scattering investigations.⁷¹ It shows that, depending on the surfactant concentration, both spherical as well as cylindrical micelles can be formed (Fig. 14 A). After adding a silica precursor, a hexagonal phase is formed without condensation of the silica precursors. The silica anions interact with the surfactant and form a silicotropic liquid crystal (SLC) (Fig. 14 B).

⁶⁹ C.Y. Chen, S.L. Burkett, H.X. Li, and M.E. Davies, *Microporous Materials* **1993** (2), 27-34.

⁷⁰ M.E. Davis, *Nature* **2002** (417), 45-49.

⁷¹ A. Firouzi, D. Kumar, L.M. Bull, T. Besier, P. Sieger, Q. Huo, S.A. Walker, and B.F. Chmelka, *Science* **1995** (267), 1138-1143.

As shown below, these SLC build SLC phases (Fig. 14 C), although the concentration of the surfactant is very low.

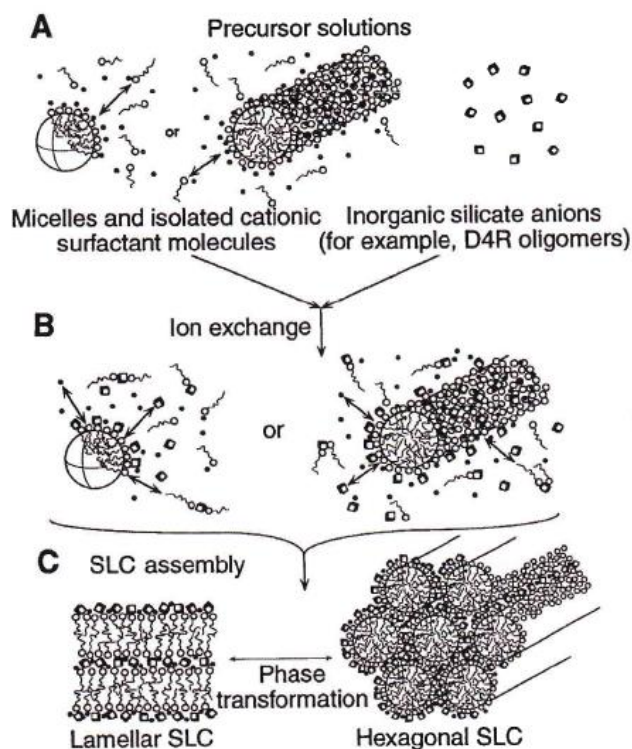


Figure 14: Formation of a SLC phase.⁷¹

1.5.3 Functionalisation Methods for Mesoporous Materials

The functionalisation of inorganic mesoporous materials with organic groups is particularly attractive, since the resulting material combines the enormous functional variation of organic chemistry with the thermal stability of inorganic chemistry. Furthermore, the inorganic and organic compounds might have properties which differ completely from those of their individual and isolated compounds.⁷²

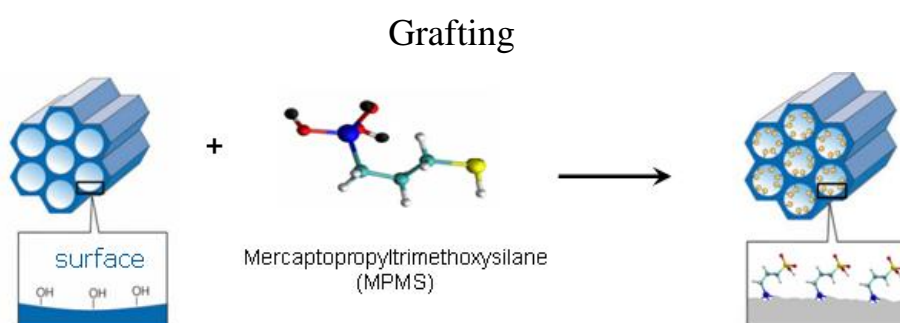


Figure 15: Grafting of mesoporous pure silica phases with MPMS and oxidation to SO_3H -groups.⁷²

Basically, two strategies are used to anchor organic groups to a structured silica surface by formation of covalent bonds: (1) subsequent modification of the pore

⁷² F. Hoffmann, M. Cornelius, J. Morell, and M. Fröba, *Angewandte Chemie Internationale Edition* **2006** (45), 44-72.

surface (grafting) or (2) simultaneous condensation of the silica source and the organosilica (co-condensation).⁷³

The grafting method refers to the subsequent modification of the inner pore surface with organic groups. Basically, alkoxy silanes of the type $(R'O)_3SiR$,⁷⁴ less frequently chlorosilanes $ClSiR_3$,⁷⁵ or aminosilanes $HN(SiR_3)_2$,⁷⁶ react with the free silanol groups on the inner or outer surface (Fig. 15). By varying the organic residue R, different organic groups can be realised. The grafting method exhibits the advantage that, after functionalisation, the mesoporous system of the starting material is usually retained. However, if the alkoxy silanes react preferentially at the pore mouth, pore blocking is especially a limiting factor and further leads to a highly inhomogeneous distribution of the functional groups, since the diffusion of further molecules into the pores is hindered.

Another serious problem that hinders the wide application of grafting to modify mesoporous silica materials is the importance of OH-groups (silanol groups) on the inner surface. Thus, many interesting and important modifications are not possible due to the absence of an alternative reactive centre.

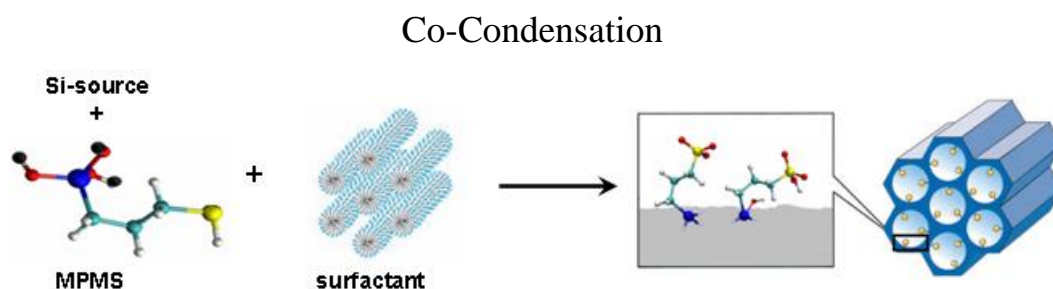


Figure 16: Co-condensation method for the organic modification of mesoporous pure silica.

An alternative way to synthesis organically modified mesoporous silica materials is the co-condensation method. Here, the alkoxy silanes of the type $(R'O)_3SiR$ are added simultaneously with a silica source (TEOS) to a solution of structure-directing surfactants, leading to materials in which the organic groups are anchored covalently inside the pore walls and are thus direct components of the silica matrix. This method has the advantage that there is no pore blocking and the organic groups are homogeneously distributed. However, there are also some disadvantages: with an increasing amount of functional groups incorporated into the silica framework, the mesoporous order decreases, which can lead to a totally disordered product. Furthermore, the amount of incorporated functional groups into the pore walls is generally lower than the amount in the starting reaction. These can be explained by

⁷³ A. Stein, B.J. Melde, and R.C. Schroden, *Advanced Materials* **2000** (12), 1403-1419.

⁷⁴ I.J. Bruce and T. Sen, *Langmuir* **2005** (21), 7029-7035.

⁷⁵ A. Sah, H.L. Castricum, A. Bliet, D.H.A. Blank, and J. Elshof, *Journal of Membrane Science* **2004** (243), 125-132.

⁷⁶ O.G. Nik, B. Nohair, and S. Kaliaguine, *Microporous and Mesoporous Materials* **2011** (143), 221-229.

the fact that $(R'O)_3SiR$ contained in the solution may homocondensate instead of cross-linking with the silica precursor.

In addition to that, an increase of organic groups leads to a reduction of pore diameter, pore volume, and surface area. Moreover, it is not possible to remove the template by simple calcination, as it is done for pure silica based materials, since this would destroy the organic functionality. Hence, only extraction methods can be used, which is more time-consuming.⁷⁷

1.5.4 Periodic Mesoporous Organosilicas

Periodic mesoporous organosilicas were first successfully synthesised in 1999 by three different independent research groups.^{78,79,80} Until that date, specific modifications of mesoporous materials with organic molecules were only realised by grafting or co-condensation. For the synthesis of organic-inorganic composite materials by hydrolysis and condensation reactions, organo-bridged R silica precursors of the type $(R'O)_3Si-R-Si(OR')_3$ were used. Hatton et al. reviewed a variety of successfully used precursors.⁸¹ In contrast to the functionalised materials prepared by grafting or co-condensation, the organic groups in the case of PMO materials are incorporated in a three-dimensional network structure inside the mesoporous walls (Fig. 17). Hence, these organic units are distributed completely homogeneously in the mesoporous matrix, their amount no longer being a limiting factor which could destroy the mesoporous structure and reduce the pore diameter or pore volume drastically. In addition to that, the presence of the organic bridges R allows a multiplicity of chemical reactions; therefore, PMO samples can be functionalised with a large array of desired groups. However, the use of organo bridged silica precursors, which exhibit sulphonic acid groups, cannot be used for the synthesis of PMO since chemical byproducts are formed due to esterification. As typical for mesoporous materials, the pore walls of PMO materials are in most cases X-ray amorphous. However, some PMO materials offer π - π interactions between the organic bridges in the walls resulting, as in the cases of benzene,⁸² ethane,⁸³ divinylbenzene,⁷² or biphenyl,⁸⁴ a crystal-like organisation of the organic bridges R within the pore walls. The powder X-ray diffraction (XRD) pattern of these PMO

⁷⁷ P.T. Tanev and T.J. Pinnavaia, *Science* **1995** (267), 865-867.

⁷⁸ S. Inagaki, S. Guan, Y. Fukushima, T. Ohsuna, and O. Terasaki, *Journal of the American Chemical Society* **1999** (121), 9611-9614.

⁷⁹ J. Melde, B.T. Holland, C.F. Blanford, and A. Stein, *Chemistry of Materials* **1999** (11), 3302-3308.

⁸⁰ T. Asefa, M.J. MacLachlan, N. Coombs, and G.A. Ozin, *Nature* **1999** (402), 867-871.

⁸¹ K. Landskron, B.D. Hatton, D.D. Perovic, and G.A. Ozin, *Science* **2003** (302), 266-269.

⁸² J.M. Knaup, P.Tölle, C. Köhler, and Th. Frauenheim, *European Physical Journal* **2009** (177), 59-67.

⁸³ W.L. Cavalcanti, R. Marschall, P. Tölle, C. Köhler, M. Wark, and Th. Frauenheim, *Fuel Cells* **2008** (8), 244-251.

⁸⁴ T. Asefa, M.J. MacLachlan, N. Coombs, and G.A. Ozin, *Nature* **1999** (402), 867-869.

materials shows reflections at small-angle regions ($2\theta \leq 10^\circ$), that are assigned to the high ordering of the mesoporous, in addition to reflections in the wide-angle range ($2\theta > 10^\circ$). This is explained by the existence of a periodicity on the molecular scale and was also confirmed by high-resolution transmission electron microscopy (HRTEM) images, which showed numerous lattice fringes along the pore axis.

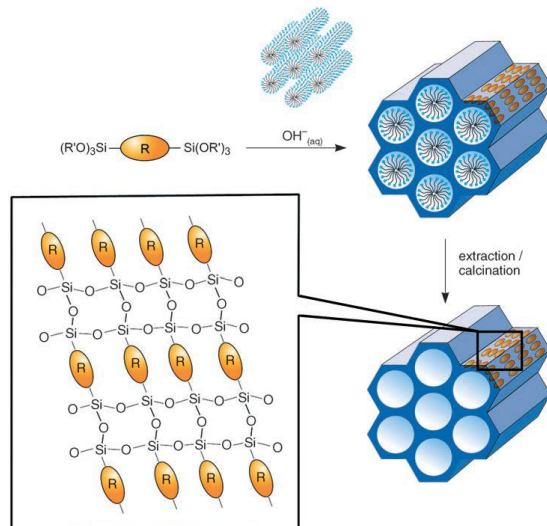


Figure 17: Synthesis of PMOs with a crystal-like arrangement of the bridging organic units R in the pore walls.⁷²

2 Proton conductivity of aluminium functionalised Si-MCM-41

2.1 Summary

Highly proton conductive additives for polymer electrolyte membrane fuel cells have already been developed by surface functionalisation of mesoporous Si-MCM-41 with sulphonic acid or imidazole groups. It is also known that zeolites, e.g. mordenite or ZSM-5, exhibit high proton conductivity with increasing temperature and decreasing Si/Al ratio.

This chapter describes the influence of Brønstedt acidic aluminium sites in the framework of mesoporous Si-MCM-41 materials on proton conductivity. Hence, some silicium atoms in the walls were substituted by aluminium. For this, different aluminium sources, i.e. sodium aluminate, aluminium sulphate and aluminium isopropoxide (AIP) were added to the synthesis gel. By adjusting the Si/Al-ratios from 8 to 40, it was found that the proton conductivity of the mesoporous aluminium silicates, measured by impedance spectroscopy, are significantly enhanced by increasing aluminium content, reaching a conductivity of $3 \cdot 10^{-3}$ S/cm at 413 K. The increase in proton conductivity compared to Al-free Si-MCM-41 results from (i) an improved hydrophilicity enhancing the water storage capability, (ii) a decreased particle size from the micrometre to the nanometre scale (50-100 nm) and (iii) the existing Brønstedt acidity in the mesoporous Al-MCM-41. The aluminium source NaAlO_2 gives clearly the best results, because the entire aluminium incorporated within the framework is tetragonally coordinated, while for samples prepared with $\text{Al}_2(\text{SO}_4)_3$ or AIP also octahedral coordination of oxygen around the aluminium centers is observed by ^{27}Al MAS NMR.

2.2 Proton conductivity of ordered mesoporous materials containing aluminium

Monir Sharifi, Roland Marschall, Martin Wilkening,
Michael Wark

Journal of Power Sources **2010** (195), 7781-7786.

<http://www.sciencedirect.com/science/article/pii/S037877530901310X>

3 Characterization of Si-MCM-41-SO₃H by SANS and MAS NMR

3.1 Summary

Mesoporous Si-MCM-41 materials functionalised by co-condensation with sulphonic acid groups exhibit the best results concerning proton conductivity and water storage at relevant temperature and low relative humidity. In order to get a deeper insight, these materials were characterized in more detail by SANS and by MAS NMR measurements.

The first article describes SANS combined with in-situ adsorption of N₂ or a H₂O/D₂O mixture (42:58) to get detailed insight into the distribution of SO₃H-groups within the pore channels, pore blocking effects, and possible structural changes of proton conducting SO₃H-functionalised Si-MCM-41. The basic idea of the experiment was the contrast matching between the silica walls and the adsorbed gases in the pores. At 298 K a H₂O/D₂O mixture of 42:58 exhibits the same neutron scattering length density (SLD) as SiO₂ and therefore quenches the diffraction signals of non-modified host material Si-MCM-41. However, in contrast to pure Si-MCM-41, the first diffraction peak of a grafted Si-MCM-41-SO₃H does not disappear completely, when the pores are filled with matching water. Hence, the H₂O/D₂O mixture, which SLD is tuned to be equal to that of SiO₂, is not able to match with walls functionalised with organic moieties. This indicates that regions with SLDs different to that of SiO₂, are present in the sample, probably predominantly at the pore mouths. For a sample functionalised by co-condensation almost no quenching of the neutron diffraction was found. This indicates that by co-condensation the entire inner pore surface is altered by functional groups, which are, thus, distributed much more homogeneously than samples functionalised by grafting. This more homogeneous distribution of SO₃H-groups also explains the higher proton conductivities.

In the second article functionalised Si-MCM-41-SO₃H samples prepared by co-condensation were investigated by MAS NMR spectroscopy and MAS PFG NMR diffusometry. ²⁹Si NMR spectra of the functionalised samples proved a successful and almost complete incorporation of mercaptopropyltrimethoxysilan (MPMS) into the mesoporous framework. The linkage between the functional group and the siliceous framework is threefold and twofold, where 31.0 % of all silicon atoms in the sample belong to T₃ groups and 5.9 % to T₂ groups. ¹³C CP MAS spectroscopy confirms that the majority of the organic functional groups remained intact after the oxidation in 30 % H₂O₂. Furthermore, only small differences of the water self-diffusion coefficient were measured by MAS PFG NMR diffusometry in opposite to the drastic changes of conductivity. The increase of conductivity (at 353 K from 9.51 to 260 · 10⁻⁵ S/cm) from 20 % to 40 % functionalisation can be explained by the reduction of the activation energy of the charge relocation in a denser lattice of proton donor sites.

3.2 Detection of homogeneous distribution of functional groups in mesoporous silica by small angle neutron scattering and in-situ adsorption of nitrogen or water

Monir Sharifi, Roland Marschall, Michaela Wilhelm, Dirk Wallacher, Michael Wark

Langmuir **2011** (27), 5516-5522.

<http://pubs.acs.org/doi/abs/10.1021/la2000188>

3.3 Detection proton conducting sulphonic acid functionalized mesoporous materials studied by impedance spectroscopy, MAS NMR spectroscopy and MAS PFG NMR diffusometry

Monir Sharifi, Michael Wark, Dieter Freude,
Jürgen Hasse

Microporous Mesoporous Mater, available online
2012.

<http://dx.doi.org/10.1016/j.micromeso.2012.02.019>

4 Investigation on proton conducting SO₃H-functionalised benzene-PMO

4.1 Summary

In previous chapters detailed investigations of proton conductance properties have been reported for Si-MCM-41 materials functionalised with sulphonic acid or aluminium groups. The benzene-PMO materials described now offer two advantages compared to Si-MCM-41; on the one hand, the presence of organic bridges allows a multiplicity of reactions and on the other hand, the crystalline pore walls open up new possibilities to form a regular distribution of anchored sulphonic acid groups.

The first article describes different routes for SO₃H-functionalisation of benzene-PMO materials. If grafting is performed at both, benzene groups and silanol groups, an ion exchange capacity (IEC) of 1.61 mmol_{H+}/g is achieved. Due to this high content of proton conducting groups combined with the flexibility of the propyl spacer, a drastic increase of proton conductivity is observed compared to pristine benzene-PMO and benzene-PMO with sulphonic acid grafted via propyl chains only on silica positions. The proton conductivity of benzene-PMO functionalized with sulphonic acid groups has been characterized using experimental and theoretical methods.

The second article within this chapter presents SANS measurements with in-situ nitrogen adsorption investigated on benzene-PMO samples. We found that by complete pore filling with nitrogen the reflection of pristine benzene-PMO at $q=0.14 \text{ \AA}^{-1}$, representing the long range order of mesopores and thus in general the contrast of wall and pore, disappears completely, while the reflections at $q=1.44 \text{ \AA}^{-1}$ and $q=1.66 \text{ \AA}^{-1}$ remain almost unchanged. This proves the molecular-scale periodicity. Furthermore benzene-PMO materials were functionalised by tethering SO₃H-groups to the surface using MPMS. With progressing N₂ adsorption the intensity of the main signal at $q \approx 0.14 \text{ \AA}^{-1}$ decreases at low adsorption levels. After capillary condensation a complete matching of the neutron scattering reflection of the main signal is obtained, since a very low functionalisation degree was achieved (0.67 mmol_{H+}/g). However, benzene-PMO functionalised with SO₃H-groups at the silica groups as well as at the benzene rings (1.61 mmol_{H+}/g) behaves differently. Nitrogen adsorption and finally, complete filling of the mesopores does not lead to any changes in the SANS patterns. This indicates that for a high degree of functionalisation with homogenous distribution of the functional groups, the SLD of SO₃H-modified benzene-PMO walls and that of adsorbed N₂ become different.

4.2 Proton conductivity of SO₃H-functionalised benzene-PMO

Monir Sharifi, Christof Köhler, Pia Tölle, Thomas Frauenheim, Michael Wark

Small **2011** (8), 1086-1097.

<http://onlinelibrary.wiley.com/doi/10.1002/sml.201001931/abstract>

4.3 Small angle neutron scattering and in-situ adsorption of nitrogen study on periodic mesoporous organosilica materials

Monir Sharifi, Dirk Wallacher, Michael Wark

Be submitted to Beilstein Journal of Nanotechnology

Small angle neutron scattering and in-situ adsorption of nitrogen study on periodic mesoporous organosilica materials

Monir Sharifi^{1,2}, Dirk Wallacher³, Michael Wark^{2*}

Address: ¹ Institute of Physical Chemistry and Electrochemistry, Leibniz University Hannover, Callinstr. 3A, D-30167 Hannover, Germany,

² Laboratory of Industrial Chemistry, Ruhr-University Bochum, Universitaetsstr. 150, D-44801 Bochum, Germany

³ Berlin Neutron Scattering Center (BENSCH), Helmholtz-Zentrum Berlin für Materialien und Energie GmbH, Hahn-Meitner-Platz 1, D-14109 Berlin, Germany

Email: Prof. Dr. Michael Wark, michael.wark@techem.ruhr-uni-bochum.de

* Corresponding author

Abstract

Periodic mesoporous materials of the type $(R'O)_3Si-R-Si(OR')_3$ with benzene as organic bridge and a crystal-like periodicity within the pore walls were investigated by small angle neutron scattering (SANS) with in-situ nitrogen adsorption at 77 K. If N_2 is adsorbed in the pores SANS measurements show, a complete matching of all the diffraction signals that are caused by the long range ordering of the mesopores in the benzene-PMO due to the fact that the benzene-PMO walls possess a neutron scattering length density (SLD) similar to those of nitrogen in the condensed state. However, signals at higher q values ($> 1 \text{ \AA}^{-1}$) resulting from the short-range order in crystal-like structures are not influenced in their SANS intensity even after complete pore filling. These experimental results confirm the assumption of a crystal-like periodicity within the PMO material walls due to π - π interactions between the organic bridges. Furthermore the SLD of pristine benzene-PMO was altered by functionalizing the surface with different amount of SO_3H -groups using the grafting method. For a low degree of functionalization ($0.81 \text{ mmol}_{SO_3H} \cdot g^{-1}$) and/or an inhomogeneous distribution of the SO_3H -groups the SLD changes only negligibly and, thus, still complete contrast matching is found. However, for higher amounts of SO_3H -groups ($1.65 \text{ mmol}_{SO_3H} \cdot g^{-1}$) being present in the mesopores complete matching of the neutron diffraction signals is not longer observed. Thus, homogeneously distributed SO_3H -groups on the inner pore walls of the benzene-PMO alter the SLD in a way that it does not longer fit to the SLD of the condensed N_2 .

Keywords

SANS, contrast matching, PMO, crystal-like periodicity, surface functionalization, distribution of functional groups

Introduction

Regarding functionalization with organic groups Si-MCM-41 often suffers from pore blocking at the pore mouth and inhomogeneous distribution of the functional groups in case of post-synthetic grafting [1-3] or, if the co-condensation route is employed, from the loss of the mesoporous structure due to a lack of optimum micelle formation with increasing the organic/functional loadings [4]. In addition a wide application of grafting to modify Si-MCM-41 materials is hindered due to the lack of reactive centers apart from the OH-groups (silanol groups) present on the inner surface [3].

Therefore periodic mesoporous organosilicas (PMOs) have attracted much attention in scientific and technological research since their discovery in 1999 by three independent groups [5-7]. PMO materials are directly forming hybrid organic-inorganic matrices by being built from precursors of the type $(R'O)_3Si-R-Si(OR')_3$ by hydrolysis and condensation reactions. The organic bridges R offer a broad spectrum of functionalities that can be incorporated into the porous framework [8]. In addition to that the organic bridge R presents reactive centers and hence a multiplicity of reactions is possible in order to modify the PMO further with a large array of desired groups. This expanded the range of applications in, for example, optical gas sensing, catalysis, chromatography, separation and nanotechnology [9]. As typical for mesoporous materials the pore walls of PMOs materials are in most cases X-ray amorphous. However, some PMO materials offer π - π interactions between the organic bridges in the walls resulting, like in the cases of benzene [10], ethene [11], divinylbenzene [12] or biphenyl [13], a crystal-like ordering of the organic bridges R within the pore walls. However, direct experimental proofs for the molecular-scale periodicity are only rarely given.

Gas sorption [14], X-ray diffraction (XRD) or IR spectroscopy [15] are commonly used as analysis tools for porous materials in order to determine structure, surface area and functionalities of the inorganic-organic materials. However, those analysis methods are only in a limited way qualified for analyzing the molecular-scale periodicity of sophisticated materials such as PMOs. Methods like XRD and gas adsorption give information on pore ordering and pore sizes but fail regarding the determination of functional groups within the pores of the host material; IR on the other hand can easily identify functional groups but is limited in analyzing the local distribution of them.

Combined techniques help to overcome these limits. Morell et al. studied the formation process of a mesoscopically ordered biphenylene-bridged organosilica with crystal-like pore walls by in situ synchrotron SAXS/XRD and demonstrated that the formation of periodicity occurs simultaneously with the formation of the mesopores as the result of a cooperative process [16]. Another advanced technique is the in-situ combination of small-angle neutron (or X-ray) scattering (SANS or SAXS) measurements with isothermal gas adsorption [17]. The intensities of the X-ray or neutron scattering reflections of the ordered porous solids are altered if the pores are filled with suitable gases. This technique is based on the so-called contrast matching, which was already introduced by Bragg et al. in 1952 [18]. The degree of matching, however, depends strongly on the chemical nature, i.e. the electron density for SAXS or the neutron scattering length density (SLD) for SANS of the pore walls in relation to the adsorbed gas. Thus, already small changes at the interface between the host material (the adsorbent) and the adsorbate can be monitored directly [19]. Smarsly et al. presented a concept to describe the subsequent stages of nitrogen sorption (i.e. micropore filling, formation of nitrogen layers and capillary condensation) for non-modified porous silica materials [20,21].

The fact that scattering in SANS measurements takes place at the nucleus, renders it superior compared to SAXS. In SANS there is a multiplicity of opportunities in the choice of the adsorbate (e.g. hydrocarbon, water, benzene, etc.), allowing tailored contrast matching experiments [18-22] and providing insight into both the sorption mechanism and the structure properties. In general adsorbates are favored where hydrogen atoms can be isotopic substituted by deuterium atoms and, hence, the coherent scattering length of condensed gas or vapor can be adjusted easily to match that of the solid host material [18]. For example, Mansour et al. showed by in-situ adsorbing suitable mixtures of H_2O/D_2O on Si-MCM-41 in a SANS equipment that the resulting population of water in the cylindrical pores after desorption at room temperature rules on a radial function with a minimum at the centre and a maximum near the pore wall [23]. By combining SANS with in situ H_2O/D_2O (42:58) adsorption at 298 K we could show that functionalization of Si-MCM-41 with SO_3H -groups by grafting leads to an inhomogeneous distribution of the groups in the pores resulting in still

strong contrast matching. Samples functionalized by co-condensation, however, exhibited almost no contrast matching, proving a very homogeneous distribution of the SO₃H-groups along the channels explaining the observed higher proton conductivities compared to grafted samples [24].

To the best of our knowledge there is only one report in literature by Mascotto et al. where peptide-functionalized benzoic acid PMO materials were investigated by SAXS/SANS with in situ gas adsorption. The authors observed a complete contrast matching with CH₂Br₂ and proved that the organic bridges R in the walls as well as the functional groups are homogeneously distributed [25]. However, they did not study the crystal-like ordering of the material.

In order to get deeper insights into the crystal-like character of PMO materials with π - π -interacting bridges we here describe for the first time in situ SANS/adsorption experiments on benzene-bridged-PMO materials showing molecular-scale periodicity performed also at q -values higher than 0.5 . Because the SLDs of N₂ in the condensed state at 77 K and SiO₂ based PMO are almost equal [24], nitrogen is a promising adsorbate to be used. Compared to H₂O/D₂O mixtures adsorption experiments with N₂ are easier to perform and especially need less time to obtain the thermodynamic adsorption equilibria.

Furthermore, pristine benzene-PMO was subsequently functionalized with SO₃H-groups; such material shows a high proton conductivity [26] and is prospective to create proton-conducting hybrid membranes for applications in fuel cells [27,28], electro dialysis for water purification [29] or photoelectrochemical cells for water splitting with solar light in order to separate the generated H₂ from the as well formed O₂ [30]. Based on functionalized mesoporous silica (e.g. Si-MCM-41-SO₃H) and different polymer materials (e.g. Nafion[®] or polysiloxanes) such type of hybrid membranes has already been realized; PMOs, however, might enhance to up to now not sufficiently high hydrothermal stability.

The functionalization of the benzene-PMO was realized by grafting using surface silanol groups as well as benzene rings to anchor the SO₃H-groups [26].

Results and Discussion

Prior to the in-situ SANS measurements the synthesized materials were investigated by nitrogen adsorption measurements in order to determine the inner surface areas, the pore volumes and the pore diameters (Fig. 1). Nitrogen adsorption on pristine benzene-PMO (-▼-) exhibits IV isotherms [32] showing shapes characteristic for the presence of mesopores; their average diameter was by DFT-based analysis determined to about 3.8 nm (Fig. 1 inset). At low relative pressures the amount of adsorbed gas first rises strongly due to monolayer adsorption followed by a continuous increase due to multilayer adsorption. A strong increase in the adsorbed amount occurs at relative pressures p/p_0 of 0.2 to 0.42 due to capillary condensation of nitrogen in the mesoporous channels. The sudden increase in the adsorption ($p/p_0 > 0.9$) for all the samples is caused by a condensation of nitrogen in the interstitial space between particles (void spaces) and cracks inside the particles. Due to the partial pore filling by anchoring propyl-SO₃H-groups on the silanol groups of the PMO by grafting the surface area, pore volume and pore diameter of benzene-PMO-0.81mmol-SO₃H (Fig.1, -●-) functionalized by grafting decrease from 952.22 m²·g⁻¹ for the pristine host material to 803.66 m²·g⁻¹, from 0.846 cm³·g⁻¹ to 0.752 cm³·g⁻¹ and from 3.8 nm to 3.5 nm, respectively.

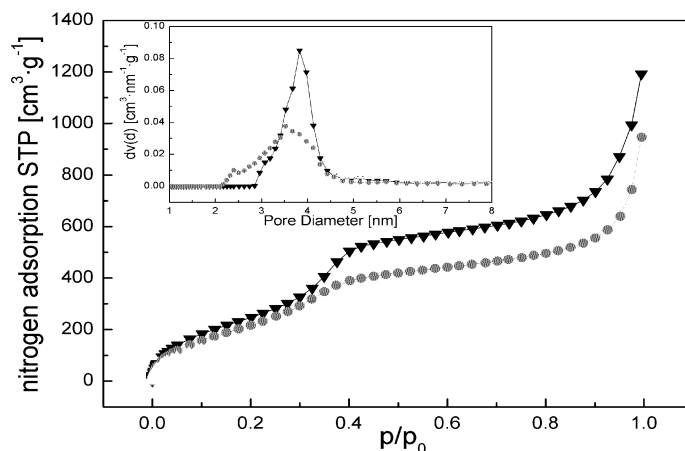


Figure 1: Nitrogen adsorption isotherms and pore diameters (inset); (- ∇ -) benzene-PMO, (- \bullet -) benzene-PMO-0.81mmol-SO₃H·g⁻¹ grafted on silica groups, (- \blacktriangle -) benzene-PMO-1.65mmol-SO₃H·g⁻¹ grafted on silica and benzene groups.

If grafting is performed at the silica (silanol) groups as well as the benzene rings resulting in a total loading of 1.65 mmol SO₃H per gram as determined by measuring the ion exchange capacity, the changes in the texture properties for modified benzene-PMO are even more pronounced, resulting in a specific surface area of 487.96 m²·g⁻¹ and a pore volume of 0.452 cm³·g⁻¹. Due to the pore filling by anchoring propyl-SO₃H-groups the high uniformity of the benzene-PMO pores is lost; especially from the sulfonation at the benzene rings an irregular distribution of pores exhibiting now diameters in the range of 2 - 4 nm (- \blacktriangle -, inset in Fig. 1) results. It is notable that the obvious difference in the isotherms of both functionalized PMO materials is not only explained by the higher loading but especially due to the harsh acidic conditions needed for sulfonation of the benzene rings. However, the mesoporous structure with hexagonal pore ordering is still well developed as shown below by SANS measurements. To clarify the general influence of the preparation conditions on the pore size distribution pure benzene-PMO materials was treated either with sulfuric acid for 12 h under reflux or with H₂O₂ (48 h). Figure S1 shows the nitrogen isotherms taken before and after the different treatments demonstrating that especially the strong acidic conditions destroy parts of the regular mesoporous network.

Figure 2 displays characteristic changes of the neutron scattering intensity for pristine benzene-PMO at different stages of nitrogen adsorption. Since no characteristic peak is shifted in position, indicating that the periodic sequence of pore-center-distance remains unchanged during the adsorption, the waterfall diagram was chosen for an easier interpretation of the measured SANS pattern. If the mesopores are empty at $p/p_0 = 0$, the presence of a hexagonal array of mesopores is indicated by a strong (100) neutron scattering peak at $q = 0.14 \text{ \AA}^{-1}$. This observation of only one reflection is in agreement with XRD measurements [5-7,33]. The intensity of this reflection is widely preserved as long as no capillary condensation takes place in the pores. During capillary condensation starting at point g of the isotherm and widely completed at point k the pores are more and more filled with nitrogen leading to almost a disappearing of intensity of the scattering reflex. After complete pore filling at $p/p_0 = 0.5$ the neutron diffraction signal is fully vanished. This complete contrast matching suggests that the SLD of the benzene-PMO framework, built-up from SiO₂ and benzene, is quite similar to that of nitrogen in the condensed phase.

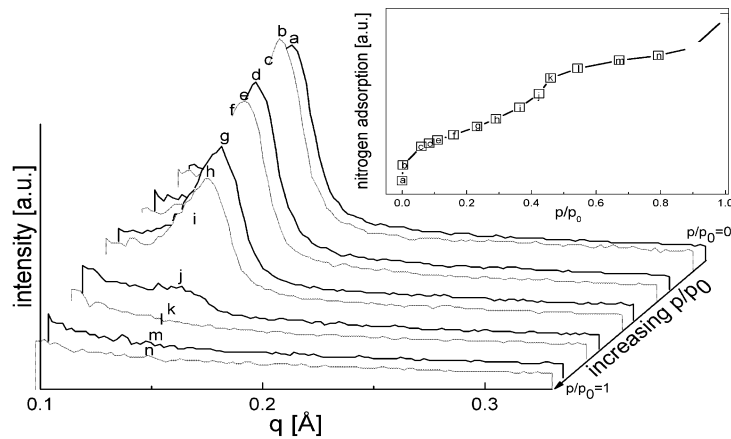


Figure 2: Neutron diffraction patterns of benzene-PMO at small q values and different amounts of adsorbed nitrogen.

The signal intensity $I(q)$ in SANS for porous materials is proportional to the square of the difference of the SLD of the host material ρ_1 and the empty pores ρ_2 , respectively.

$$I(q) \sim k(\rho_1 - \rho_2)^2 = k(\Delta \rho)^2 \quad (1)$$

$$I(q) \sim k(\rho_{\text{solid}})^2, \text{ if } \rho_{\text{solid}} \gg \rho_{\text{evacuated}} \quad (2)$$

with k being a constant depending on $P(q)$, a form factor of the pores which is determined by the shapes of the individual pores, and $S(q)$ which results from the correlation function of the pores [34]. The scattering length densities of amorphous silica ($\rho_{\text{SiO}_2} = 3.43 \cdot 10^{10} \text{ cm}^{-2}$) and liquid nitrogen at 77 K ($\rho_{\text{N}_2} = 3.23 \cdot 10^{10} \text{ cm}^{-2}$) are almost equal [35]. However, the mesoporous framework of benzene-PMO consists not only of SiO_2 but also of organic benzene groups. Thus, since no literature data is available for PMO materials yet, the exact scattering length density must be calculated for further interpretation.

The scattering potential of the nucleus of an individual atom is described by the scattering length b indicating neutron-nucleus-interaction. The scattering length density ρ_{SLD} is defined by the sum of the scattering lengths of all atoms which are involved in the molecular structure divided by the molecule volume:

$$\rho_{\text{SLD}} = \sum_{i=1}^N b_i N_i \frac{\rho_0 N_A}{M} \quad (3)$$

N_A : Avogadro constant, M : mass of the used formula unit, e.g. $\text{Si}_2\text{O}_2\text{C}_6\text{H}_4$ ($M=164 \text{ g}\cdot\text{mol}^{-1}$) for the SLD calculation for pure benzene-PMO, b_i : scattering length of atom i , N_i : number of atoms of sort i in the formula unit and ρ_0 the density [36,37]. For the SLD-calculation of the present material the atomic scattering lengths of $b_C = 6.648 \text{ fm}$, $b_H = -3.741 \text{ fm}$, $b_{\text{Si}} = 4.151 \text{ fm}$, $b_S = 2.874 \text{ fm}$ and $b_O = 5.805 \text{ fm}$ were used [36]. To determine the density ρ_0 of each mesoporous material the Archimedean principle was used; the results are given in Table 1. The SLD for $1.65 \text{ mmol SO}_3\text{H g}^{-1}$ functionalized benzene-PMO was calculated considering in the formula unit that the mesoporous surface is altered homogeneously by $1.42 \text{ mmol SO}_3\text{H g}^{-1}$ attached to the benzene bridges and inhomogeneously by $0.23 \text{ mmol propyl-SO}_3\text{H}\cdot\text{g}^{-1}$ attached to Si-groups, respectively. The formula of a unit cell is $\text{Si}_2\text{O}_2\text{C}_6\text{H}_4(\text{C}_3\text{H}_7\text{SO}_3)_{1/24}(\text{SO}_3\text{H})_{1/4}$. The mesoporous surface of $0.81 \text{ mmol SO}_3\text{H}\cdot\text{g}^{-1}$ functionalized benzene-PMO prepared according the synthesis route was obtained considering that the functional groups are altered inhomogeneously mainly at the pore mouths [24]. Under this assumption in which the functional groups do not reach the inner pore surface, the SLD is only influenced by the density but not by the amount of functional groups resulting a value of $3.84 \cdot 10^{10} \text{ cm}^{-2}$.

Opposite to that, the SLD was also calculated for the same sample with the assumption that the functional groups are distributed homogenously and hence must be considered in the formula unit, i.e. $\text{Si}_2\text{O}_2\text{C}_6\text{H}_4(\text{C}_3\text{H}_7\text{SO}_3)_{1/7}$. The result given in the bracket in Tab. 1 does not differ much from that of the first assumption.

Table 1: Structural data and ion exchange capacities (IEC) of SO_3H -functionalized benzene-PMO materials.

Sample	SLD [$10^{10} \cdot \text{cm}^{-2}$]	Density [$\text{cm}^3 \cdot \text{g}^{-1}$]
benzene-PMO	3.62	2.38
benzene-PMO-0.81mmol $\text{SO}_3\text{H g}^{-1}$, grafted on silica groups	3.84-(3.91)	2.41
benzene-PMO-1.65mmol $\text{SO}_3\text{H g}^{-1}$, grafted on the silica and the benzene groups	4.55	2.69
Nitrogen	3.23	0.807

As explained in equations (1) and (2) for further interpretation the assumption of a two-phase-system was made, where each phase differs only in its SLD although it might consist of several compounds. Phase one consists of the benzene-PMO framework and condensed nitrogen (relates to ρ_1 in equation 1) and phase two consists of empty pores (relates to ρ_2 in equation 1), since both phases exhibit a different SLD for all stages of adsorption. As long as the assumption for ρ_1 holds, the reflections of benzene-PMO are erased in SANS measurements if all pores are filled with N_2 and no inaccessible pores remain empty [20]. However, also for completely filled pores a diffraction signal can remain, if the SLD of the framework was altered from that of the adsorbate, i.e. the assumption for ρ_1 does not hold. As already shown in Tab. 1 for benzene-PMO-1.65mmol- $\text{SO}_3\text{H g}^{-1}$, grafted on the silica and the benzene bridges, ρ_1 for the framework strongly increases due to the introduction of the functional groups. Thereby the SO_3H -groups directly at the benzene rings have a much stronger effect than the propyl- SO_3H groups at the silica groups.

Small amounts of adsorbed nitrogen in pristine benzene-PMO show significant particularities as shown by the SANS curves in Fig. 2. The intensity of the main reflection at $q = 0.14 \text{ \AA}^{-1}$ increases at a relative pressure of $p/p_0 = 0.06$ due to the filling of voids with condensed nitrogen which smoothes the rough inner pore surfaces, i.e. some irregularities in the pore wall thickness, which might maintain after template extraction [17,37]. As a consequence the intensity of the main reflection increases since the periodicity is improved. Further adsorption of nitrogen results in a continuous decrease of the neutron scattering reflection at $q = 0.14 \text{ \AA}^{-1}$ in agreement with equation (1) and the assumption of a two-phase-system. At capillary condensation conditions, i.e. at relative pressures $p/p_0 > 0.26$, the SANS reflection intensity $I(q)$ drops drastically due to N_2 condensation in the pores. After complete capillary condensation at a relative pressure of $p/p_0 \approx 0.50$ scattering signals at small q -values are no longer observed (Fig. 2). Because of the homogenous incorporation of organic groups as bridges between two Si atoms in the mesoporous framework Inagaki and co-workers found XRD reflexes at high 2θ angles for mesoporous benzene-PMO [5]. Figure 3 shows that analogues to XRD measurements neutron scattering exhibit one quite sharp reflection at $q = 1.66 \text{ \AA}^{-1}$ and a very broad reflection at $q = 1.44 \text{ \AA}^{-1}$, respectively, resulting from the periodic arrangement of the benzene groups along the channel direction. In contrast to the totally disappearing reflection at $q = 0.14 \text{ \AA}^{-1}$, representing the long range order of the mesopores and thus in general the density contrast between wall and pore, these reflection at $q = 1.44 \text{ \AA}^{-1}$ and $q = 1.66 \text{ \AA}^{-1}$, reflecting the molecular-scale periodicity in the walls, remain almost unchanged after complete filling the pores with nitrogen (inset Fig. 3). This proves undoubtedly the crystal-like pore wall structure of porous PMO materials, and underlines the results found by analyses XRD measurements [5,7,16].

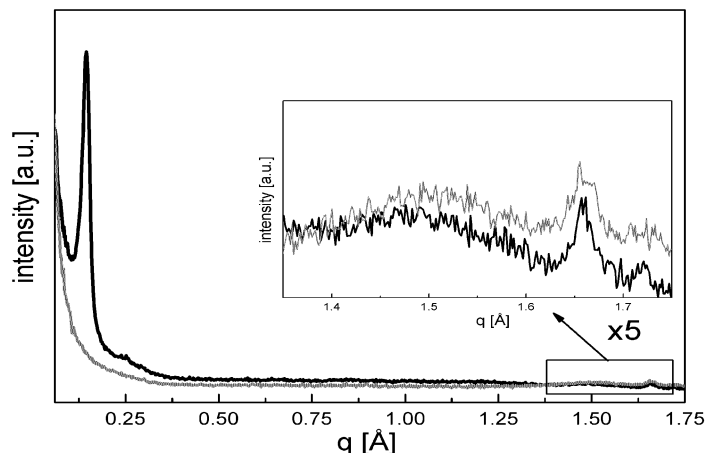


Figure 3: Neutron diffraction patterns of benzene-PMO at small and high q values for empty (black curves) and nitrogen filled pores (red curves).

Figure 4 shows neutron scattering curves of functionalized mesoporous benzene-PMO- $0.81\text{mmol-SO}_3\text{H}\cdot\text{g}^{-1}$ synthesized by anchoring SO_3H -groups via propyl chains on silica groups in dependence on the equilibrium partial pressures of nitrogen adsorbed to the pores. With this synthesis route a proton exchange capacity of only $0.81\text{mmol}_{\text{H}^+}\text{g}^{-1}$ or $0.81\text{mmol SO}_3\text{H}$ -groups per gram material was achieved. In agreement with results from nitrogen adsorption (Fig. 1) the presence of the main reflection peak in the obtained neutron diffraction pattern in vacuum confirms that the mesoporous structure of benzene-PMO- $0.81\text{mmol-SO}_3\text{H}\cdot\text{g}^{-1}$ is preserved after the grafting procedure. With continuous nitrogen adsorption the sample exhibits analogue results to pristine benzene-PMO (Fig. 3), as the intensity of the main signal at $q \approx 0.14\text{Å}^{-1}$ decreases only weakly at low adsorption levels. Once condensation takes place at relative pressures of $p/p_0 \geq 0.22$ (inset in Fig. 4) a faster decrease of the main signal in the neutron scattering reflection is obtained. After complete pore filling the hexagonal pore structure gets invisible for neutron scattering indicating that the SLD of the walls of $0.81\text{mmol-SO}_3\text{H}$ -functionalized benzene-PMO formed according to this synthesis route differs not significantly from that of pristine benzene-PMO. This result is in agreement with literature data for comparable Si-MCM-41 materials showing that grafting with quite bulky silanes, as the MPMS, often leads to an inhomogeneous distribution of functional groups [24,33] as seen also by the low decrease in mesopore volume.

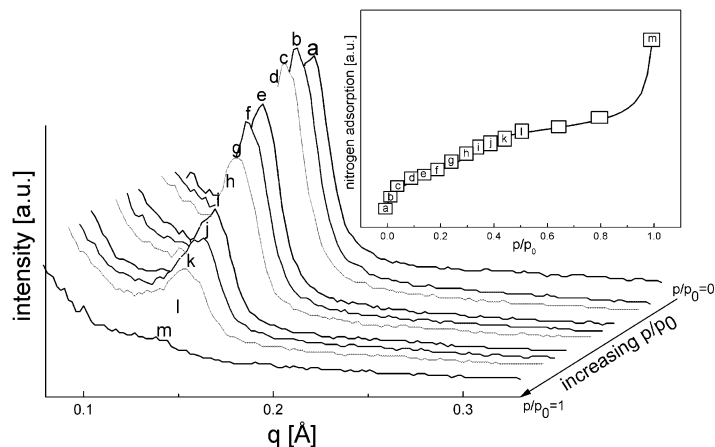


Figure 4: Neutron diffraction patterns of MPMS functionalized benzene-PMO-0.81mmol-SO₃H·g⁻¹ grafted on silica groups at small q values at different stages of adsorbed nitrogen.

Benzene-PMO with higher degree of functionalization can be achieved by additional modification at the benzene rings. Thus, a maximum SO₃H-loading with an ion-exchange capacity of 1.65 mmol_{H⁺} g⁻¹ was achieved. The neutron scattering reflex found at low q values in vacuum for this material (Fig. 5) confirms the existence of ordered mesoporous structure as also found by nitrogen adsorption measurements (compare Fig. 1). However, unambiguously the strong acid conditions present during this functionalization procedure (compare to Fig. S1) reduce the quality of the mesoporous structure as indicated by a broadening of the SANS signal and a decrease in intensity (Fig. 5) compared to that of the sample functionalized only at the silica. Nevertheless, adsorption of N₂ alters the reflex intensity and, thus, allows conclusions on the chemical nature of the mesopores. Again, the intensity of the main reflection decreases while a small amount of nitrogen is adsorbed (Fig. 5). A maximum decrease of 21% in intensity is achieved after capillary condensation at relative pressure $p/p_0 > 0.4$. Thus, completely filling of the mesopores does not much alter the SANS patterns. Again the reflections at $q = 1.66 \text{ \AA}^{-1}$ and 1.44 \AA^{-1} resulting from the periodic arrangement in the walls are still present and show, as expected, no changes in intensity after complete pore filling (Supporting Information, Figure S2).

Hence, only weak matching of the neutron diffraction signal was found for benzene-PMO-1.65mmol-SO₃H g⁻¹ with a maximum loading of functional groups. This indicates that by functionalization, at the silica groups as well as the benzene rings, at least about 80 % of the entire inner pore surface is altered by functional groups which are, thus, much more homogeneously distributed than in samples only functionalized by grafting at the silanol groups [6,7]. As a result in almost the whole mesoporous framework the SLD of the adsorbed nitrogen is different from that of the (modified) pore walls impeding contrast matching. Analogue results were found for homogeneously SO₃H-modified Si-MCM-41 (co-condensation route) by SANS measurements with in situ adsorption of a H₂O/D₂O mixture for which a composition was used which tunes the SLD to be equal to that of SiO₂ [24].

Hence, the assumption of a two-phase-system, which was made in previous for pure benzene-PMO and benzene-PMO-0.81 mmol-SO₃H g⁻¹ with low loading, is not holding anymore for benzene-PMO-1.65mmol-SO₃H·g⁻¹ functionalized at both silica groups and benzene rings. The homogenous distribution of SO₃H-groups on the inner surface of the porous materials is not achieved by the reaction of MPMS at silanol groups, which exclusively appear on the first accessible silanol close to the pore mouths but by the sulfonation at the benzene rings.

Modifications at the stable benzene rings are in general kinetically hindered which ensures that the $\text{SO}_3\text{H}/\text{H}_2\text{SO}_4$ solution used for the functionalization first spreads uniformly in the whole pore network before significant reaction at the benzene rings in the walls takes place.

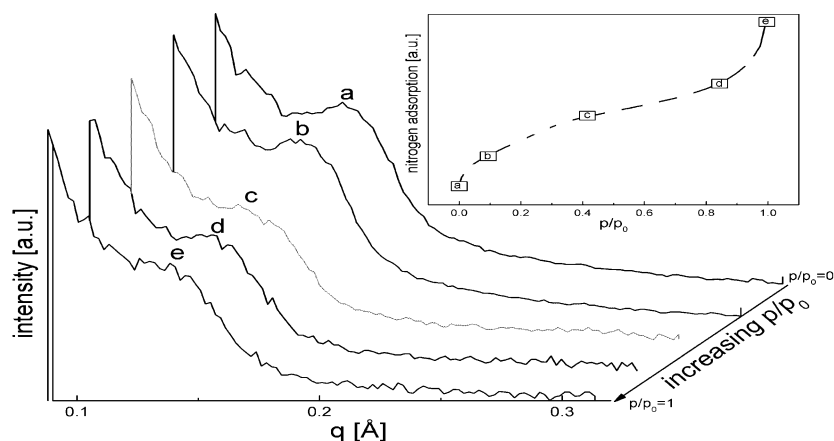


Figure 5: Neutron diffraction patterns of functionalized benzene-PMO with $1.65\text{mmol-SO}_3\text{H g}^{-1}$ grafted on benzene rings and on silica at small q values at different stages of nitrogen adsorption.

Conclusion

SANS measurements combined with in-situ adsorption of nitrogen at 77 K were used to characterize pristine benzene-PMO and different functionalized benzene-PMO materials prepared by grafting SO_3H -groups on silica and at benzene groups, respectively. The obtained neutron diffraction patterns demonstrated that N_2 matches completely all signals of pristine benzene-PMO that are caused by the long range ordering of the mesopores. Simultaneously signals at higher q values were not influence by the pore filling. Hence in addition to XRD pattern another experimental prove is given for the crystal-like periodicity of the synthesized benzene-PMO materials. In addition to that SLD calculation of porous material are reported in this study and confirmed by SANS contrast matching measurements. Furthermore, the SLD of pure benzene-PMO was altered by introducing different amounts of SO_3H -groups. The resulting neutron diffraction patterns showed that small amounts of SO_3H -groups ($0.81\text{ mmol-SO}_3\text{H-g}^{-1}$) that were anchored via propyl linkers mainly at the pore mouths only negligibly change the SLD, and complete signal matching by N_2 is still obtained. However, a higher degree of functionalization with SO_3H -groups ($1.65\text{ mmol-SO}_3\text{H-g}^{-1}$) anchored at silica groups as well as at benzene groups on the surface hinders complete matching indicating a homogenous distribution of functional groups. SLD calculations show that in particular the SO_3H anchored without any spacer directly at the benzene rings change the neutron scattering behavior of the framework.

Experimental

Synthesis of benzene-PMO: Ordered mesoporous benzene-PMO was synthesized by adding 7.49 g octadecyl-trimethylammoniumchloride surfactant to 225 mL distilled water and 14.4 mL NaOH (6M) at 328 K [1]. After a clear solution was obtained, 9 g 1,4-bis(triethoxysilyl)benzene (BTEB) were added to the surfactant solution at room temperature under vigorous stirring. The mixture was treated ultrasonically for 20 min to disperse the hydrophobic BTEB in the aqueous solution. Afterwards the dispersion was stirred for 20 h at

room temperature and kept 24 h at 368 K under static conditions. The resulting white solid was filtered and washed with water and ethanol. The surfactant was removed by extraction in 250 mL ethanol with 7.5 mL 36% HCl at 353 K for 24 h.

Synthesis of benzene-PMO-SO₃H, SO₃H-groups grafted on silica: 0.5 g benzene-PMO were given into a flask and dried under vacuum for 3 h. Under argon atmosphere the white powder was suspended in 20 mL dry toluene. Afterwards 1.2 mL 3-mercaptopropyltrimethoxysilane (MPMS) were added and the suspension was heated under reflux up to 383 K. The reaction mixture was stirred for 24 h followed by filtration and washing with toluene and ethanol. In order to obtain SO₃H-groups the attached SH-groups were oxidized with hydrogen peroxide. Therefore 0.3 g of the MPMS functionalized sample prepared by grafting were suspended in 10 mL of H₂O₂ solution (30 wt.-%) and stirred for 48 h at room temperature. The powder was filtered and washed with ethanol and water. Then the oxidized solid was suspended in 30 mL of a 2 M H₂SO₄ solution, stirred for 2 h at room temperature and finally filtered and washed with ethanol and water.

Synthesis of benzene-PMO-SO₃H, SO₃H-groups grafted on benzene rings and on silica: 0.8 g benzene-PMO were dried under vacuum for 3 h. Afterwards 50 mL of a 25% SO₃H/H₂SO₄ solution were added under argon atmosphere. The dispersed solution was heated to 378 K and kept at that temperature for 10 h under reflux. The resulting solid exhibits 1.42 mmol SO₃H-groups per g, which was determined by titration was filtrated and washed with 3 L water. Afterwards 0.5 g of the sulfonated material was functionalized by grafting with MPMS as described before. Finally, the solid was stirred for 2 h in 30 mL HCl to protonate and form sulfonic acid groups resulting in a maximum loading of 1.65 mmol SO₃H-groups per g.

Characterization

Neutron diffraction patterns with in-situ gas adsorption were collected at the V1 diffractometer of the cold neutron source ($\lambda = 5.23\text{\AA}$) of the BER-II reactor located at the Helmholtz Center Berlin (HZB). The scattering intensity was collected in the range of $q = 0.01\text{--}0.7\text{ \AA}^{-1}$ by varying detector position at a sample-to-detector distance of 102.52 cm. The scattering vector q is defined as $q = 4\pi/\lambda \sin(\theta)$, with λ being the wavelength and θ the Bragg angle. The temperature during neutron experiments was 77 K. Before measuring each neutron scattering pattern, the sample was filled with a certain amount (n/n_0) of adsorptive, by applying a gas adsorption setup which was connected to the measuring cell and enables a direct in situ SANS measurement for each point of the p-V adsorption isotherm. SANS measurements were only performed after a constant cell pressure was given which ensures an adsorption equilibration. Nitrogen adsorption isotherms at 77 K were determined on a Quantachrome Autosorb 3 apparatus. Prior to each adsorption measurement, the samples were outgassed at 433 K for 24 h. The Brunauer-Emmett-Teller (BET) method was used to determine the specific surface area. The pore volumes and pore diameters were calculated according to the density functional theory (DFT) [31].

In order to determine the density of pure and SO₃H-functionalized benzene-PMO materials the Archimedean principle was used. Thus, each sample was pressed as pellet and dried in an oven at 373 K for 48 h before weighing in air. After that each sample was soaked into the impregnation solution prior to another weighing by using a hydrostatic balance. Hereby, it is important that the sample was immersed completely into the impregnation solution.

The loading with exchangeable H⁺ ions was determined by titration with NaOH(1M), resulting in 0.81 mmol_{SO₃H}·g⁻¹ if SO₃H-groups were grafted on silica and 1.65 mmol_{SO₃H}·g⁻¹ if SO₃H-groups were grafted on silica and benzene rings, respectively.

Supporting Information

Supporting information features nitrogen isotherms and pore diameter of benzene-PMO taken before and after the different acidic treatments conditions (Fig. S1). SANS diffraction patterns of functionalized benzene-PMO with 1.65mmol-SO₃H-groups grafted on benzene rings and silica groups after complete pore filling with nitrogen are shown in Fig. S2.

Acknowledgements

The work was supported by the Deutsche Forschungsgemeinschaft (DFG) (WA 1116/15, SPP 1181) by the European Commission under the 6th Framework Programme through the Key Action: Strengthening the European Research Infra-structures (RII3-CT-2003-505925 NMI 3). The authors thank Dr. Thomas Hauß and Nico Grimm (Helmholtz-Zentrum Berlin für Materialien und Energie GmbH, Berlin, Germany) for technical support during the SANS measurements and Prof. Jürgen Caro (Institute of Physical Chemistry and Electrochemistry, Leibniz University Hannover, Germany) for general support.

References

- 1 Taguchi A.; Schüth F. *Micropor. Mesopor. Mat.* **2005**, *77*, 1–45.
- 2 Jones C. W.; Tsuji K.; Davis M. E. *Nature* **1998**, *66*, 52–54.
- 3 Hoffmann F.; Cornelius M.; Morell J.; Fröba M. *Angew. Chem. Int. Ed.* **2006**, *45*, 3216–3251.
- 4 Gartmann N.; Brühwiler D. *Angew. Chem., Int. Ed.* **2009**, *48*, 6354–6354.
- 5 Inagaki S.; Guan S.; Fukushima Y.; Ohsuna T.; Terasaki O. *J. Am. Chem. Soc.* **1999**, *121*, 9611–9614.
- 6 Melde B. J.; Holland B. T.; Blanford C. F.; Stein A. *Chem. Mater.* **1999**, *11*, 3302–3308.
- 7 Asefa T.; MacLachlan M. J.; Coombs N.; Ozin G.A. *Nature* **1999**, *402*, 867–871.
- 8 Fujita S.; Inagaki S. *Chem. Mater.* **2008**, *20*, 891–908.
- 9 Soler-Illia G. J.; Sanchez C.; Lebeau B. *J. Chem. Rev.* **2002**, *102*, 4093–4138.
- 10 Bion N.; Ferreira P.; Valente A.; Gonçálves I. S.; Rocha J. *J. Mater. Chem.* **2003**, *13*, 1910–1913.
- 11 Nakajima K.; Tomita I.; Hara M.; Hayashi S.; Domen K.; Kondo J. N. *Catalysis Today* **2006**, *11*, 6151–6159.
- 12 Boury B.; Corriu R. J. P.; Le Strat V.; Delord P.; Nobili N. *Angew. Chem., Int. Ed.*, **1999**, *38*, 3172–3175.
- 13 Boury B.; Ben F.; Corriu R. J. P.; Delord P.; Nobili M.; *Chem. Mater.* **2002**, *14*, 730–738.
- 14 Kruk M.; Jaroniec M.; Sayari A. *Langmuir* **1997**, *13*, 6267–6273.
- 15 Kumar D.; Schumacher K.; Du Fresne von Hohenesche C.; Grün M.; Unger K. K. *Colloids and Surfaces A: Physicochem. Eng., Aspects* **2001**, *187*, 109–116.
- 16 Morell J.; Cilaine V.; Cornelius M.; Rebbin V.; Tiemann M.; Amenitsch H.; Fröba M.; Lindén M. *Chem. Mater.* **2004**, *16*, 5564–5566.
- 17 Tun Z.; Mason P.C.; Mansour F.K.; Peemoeller H. *Langmuir* **2002**, *18*, 975–977.
- 18 Ramsay J. D. F.; Wing G. *J. Coll. Interf. Sci.* **1991**, *141*, 475–485.
- 19 Smarsly B.; Thommes M.; Ravikovitch P. I.; Neimark A. V. *Adsorption* **2005**, *11*, 653–655.
- 20 Smarsly B.; Göltner C.; Antonietti M.; Ruland W.; Hoinkis E. *J. Phys. Chem. B* **2001**, *105*, 831–840.
- 21 Sel O.; Brandt A.; Wallacher D.; Thommes M.; Smarsly B. *Langmuir* **2007**, *23*, 4724–4727.

- 22 Bragg W. L.; Perutz M. F. *Acta Cryst.* **1952**, *5*, 277–283.
- 23 Mansour F. K.; Peemoeller H. *Langmuir* **2002**, *18*, 975–977.
- 24 Sharifi M.; Marschall R.; Wilhelm M.; Wallacher D.; Wark M. *Langmuir* **2011**, *27*, 5516–5522.
- 25 Mascotto S.; Wallacher D.; Kuschel A.; Polarz S.; Zickler G.A.; Timmann A.; Smarsly B. *Langmuir* **2010**, *26*, 6583–6592.
- 26 Sharifi M.; Köhler C.; Tölle P.; Frauenheim T.; Wark M. *Small* **2011**, *7*, 1086–1097.
- 27 Wilhelm M.; Jeske M.; Marschall R.; Cavalcanti W.; Tölle P.; Köhler C.; Koch D.; Frauenheim T.; Grathwohl G.; Caro J.; Wark M. *J. Membr. Sci.* **2008**, *316*, 164–175.
- 28 Choi Y.; Kim Y.; Kim H.K.; Lee J.S. *J. Membr. Sci.* **2010**, *357*, 199–205.
- 29 Klaysom C.; Marschall R.; Wang L.; Ladewig B.P.; Lu G.Q. *J. Mater. Chem.* **2010**, *20*, 4669–4674.
- 30 Seger B.; Kamat P.V. *J Phys Chem C* **2009**, *113*, 18946–18952.
- 31 El-Merraoui M.; Aoshima M.; Kaneko K. *Langmuir* **2000**, *16*, 4300–4304.
- 32 Zhao X.S.; Lu G.Q. *J. Phys. Chem. B*, **1998**, *102*, 1556–1561.
- 33 Brühwiler D. *Nanoscale*, **2010**, *2*, 887–892.
- 34 Li J.C.; Ross D.K.; Howe L.D.; Heeman R.; Ibel R. *Phys. Rev. B*, **1994**, *49*, 5911–5916.
- 35 Ramsay J.D.F.; Kallus S. *J. Non-Crystalline Solids*, **2001**, *285*, 142–147.
- 36 Prinz D., Die Porenstruktur von Kohlen, Rheinisch-Westfälischen Technischen Hochschule, Dissertation. Aachen, **2004**.
- 37 Bellissent R.; Descotes L.; Bouc F.; Pfeuty P. *Phys.* **1990**, *41*, 2135–2139.

5 Enhanced proton conductivity by more appropriate functional groups and oxidation methods

5.1 Summary

This chapter presents studies on TESP functionalised Si-MCM-41 materials that were oxidized in the absence of any catalyst or solvent with different oxidising agents: Br_2 , H_2O_2 or HNO_3 in order to find an optimum oxidising agent for transferring sulphur containing compounds attached within the mesopore channels into SO_3H -groups with a maximum yield.

The amount of sulphonic acid groups, which are finally anchored by organic linkages on the mesoporous surface prepared by the co-condensation method were determined by ion exchange capacity.

It is shown that H_2O_2 , which is dominantly used in organic chemistry for such type of reactions, exhibits a insufficient yield of only 80 % followed by HNO_3 (66 %). Only with Br_2 , being a non-typical oxidation agent, a surpassing yield of SO_3H -groups was obtained (98 %) exceeding even those of reactions employing catalysts or solvents.

Impedance spectroscopy measurements prove that proton conductivities of the loaded samples are extremely high confirming the high content of SO_3H -groups. This was achieved by complete oxidation of all sulphur precursors, as well as by their uniform distribution in the pore channels.

5.2 Investigation on the optimal oxidation agent for a maximum yield of sulphonic acid groups in MCM-41

Monir Sharifi, Jenny Schneider, Michael Wark

Microporous Mesoporous Mater, **2012** (115) 506-510.

<http://www.sciencedirect.com/science/article/pii/S1387181111004781>

6 Closing Remarks

This work is focused on the synthesis and characterization of functionalised mesoporous materials, based on Si-MCM-41 and benzene-PMO. As described in Chapter 2-5 these materials were modified with sulphonic acid groups since the resulting products exhibit the best results concerning proton conductivity and water storage at relevant temperature and low relative humidity. These materials are promising candidates for composite organic-inorganic membranes in the field of fuel cells. This technology is one of today's greatest research fields due to climate change and shortage of resources.

Beside the functionalisation with organic groups it is very useful to improve the inorganic mesoporous framework, as shown in Chapter 2 by the introduction of Brønstedt acidic. The Al-MCM-41 materials exhibit enhanced properties in proton conductivity and water storage. The aluminium source NaAlO₂ showed clearly the best results, because all aluminium within the framework is tetrahedrally coordinated. For samples with Si/Al ratio of 10 where Al-content and quality of the mesoporous structure are in optimum balance, samples showed conductivities of about $3 \cdot 10^{-3}$ S/cm at 413 K. Thus, compared to pristine Si-MCM-41 an enhanced starting material for further functionalisation with organic groups is presented. However, a typical modification with MPMS is hindered, since the subsequent oxidation of the thiol groups into proton conducting sulphonic acid groups removes the incorporated aluminium. One approach to avoid this problem might be the use of TESP or TESPT instead of MPMS. The functionalisation can be performed analogue to MPMS by grafting or co-condensation. However, the use of H₂O₂ is no longer mandatory, since Br₂ can be used to transfer the di- or tetrasulfide into sulphonic acid groups, respectively. Thus, the strong acid condition of a H₂O₂ oxidation can be avoided.

We found out that samples synthesised by co-condensation exhibit higher proton conductivities compared to those obtained by the grafting method with same loadings. Thus, for further insight SANS experiments combined with in-situ adsorption of a H₂O/D₂O mixture (42:58, at 298 K) were used to describe pristine mesoporous Si-MCM-41 and especially proton conducting SO₃H-functionalised Si-MCM-41. In contrast to pure Si-MCM-41 the first diffraction peak decreased obviously, but did not disappear completely even after complete pore filling. This indicated that regions with neutron scatter lengths different to that of SiO₂ are present. For a sample functionalised by co-condensation almost no quenching of the neutron diffraction was found. This shows that here all regions of the pores are altered by the functional groups proving that the loading is much more homogeneous than with grafting by what the functional groups are only anchored at the pore entrances. The more homogeneous distribution of groups after co-condensation explains the higher proton conductivities observed.

However, the grafting method is in some case very important to achieve higher loadings of proton conducting groups. In this thesis MPMS or TESPDP were used for the co-condensation. Thus the proton conducting groups were anchored via propyl-chains to the mesoporous surface. The use of organic compounds with short chain length (methyl instead of propyl) for the co-condensation might be advantageous since the hydroxyl groups on the inner pore surface would be more easily accessible for other molecules. Thereby additional grafting with further organic groups would be possible increasing the total loading. However, in the case of MPMS or TESPDP functionalised samples the long propyl-chains would hinder an additional grafting.

Although different characterization methods (XRD, gas adsorption, IR, EDXS, IEC, IS, SANS) were performed on MPMS functionalised materials, only with solid state NMR measurements a clear evidence for the successful incorporation of MPMS and its oxidation was given. ^{13}C CP MAS NMR spectra show three signals of the functional group $\equiv\text{Si-CH}_2\text{-CH}_2\text{-CH}_2\text{-SO}_3\text{H}$ with chemical shift of 11 ppm, 18 ppm and 54 ppm, respectively. This confirms that the majority of the carbon species build the desired functional group ($-\text{SiC}_3\text{H}_6\text{SO}_3\text{H}$). ^{29}Si NMR spectra of the functionalised samples proved a successful and almost complete incorporation of MPMS into the mesoporous framework. The linkage between the functional group and the siliceous framework is threefold and twofold.

As already mentioned proton conducting benzene-PMO with crystal-like periodicity within the pore walls were synthesised as an alternative starting material. For grafting SO_3H -groups to the benzene ring a loading of $1.42 \text{ mmol}_{\text{H}^+}/\text{g}$ is reported, which exceeds the best value for grafting on Si-MCM-41 substrate. If grafting is performed at both benzene groups and silanol groups ($\text{IEC} = 1.61 \text{ mmol}_{\text{H}^+}/\text{g}$), a dramatic increase of proton conductivity, compared to pristine benzene-PMO and benzene-PMO with sulphonic acid grafted via propyl chains only on silica positions, is observed. From theoretical calculations it was shown that that protonation of an isolated sulphonic acid group is energetically favourable explaining the high proton conductivity. However, the loading with proton conducting groups could not be further increased, although in contrast to Si-MCM-41, two reactive centres were used to anchor sulphonic acid groups: silanol groups and benzene groups. For that reason functionalisation of PMO materials by the co-condensation method is required, since higher loading can be achieved and additional to that the organic bridge can be used for further loading. First experiments show that the relation of the condensation times of the used PMO precursor $(\text{R}'\text{O})_3\text{Si-R-Si}(\text{OR}')_3$ and that of the silane bearing the functional group (MPMS, MPES) is the key factor. Hence, the incorporation of MPMS in an ethane-PMO framework was only successful when both components start condensation at the same time. Another approach for the synthesis of high proton conducting PMO materials with high amount of sulphonic acid group might be the use of precursors of the type $(\text{R}'\text{O})_3\text{Si-R-Si}(\text{OR}')_3$ with $\text{R} = (\text{CH}_2)_x\text{-S}_2\text{-(CH}_2)_x$.

Thus, a maximum amount of sulphur is available for subsequent transformation into sulphonic acid groups. This oxidation mechanism involves a S-S bond-breaking as shown by the oxidization of TESPDP functionalised Si-MCM-41. Hereby, different oxidation agents (Br_2 , H_2O_2 or HNO_3) were used in order to find a maximum yield for the transformation of sulphur containing compounds into SO_3H -groups. We found that H_2O_2 , which is dominantly used in organic chemistry for such type of reactions, exhibits a insufficient yield of only 80% followed by HNO_3 (66%). Only with Br_2 , being a non-typical oxidising agent, a surpassing yield of SO_3H -groups was obtained (98%) exceeding even those of reactions employing catalysts or solvents. However, in the case of TESPDP-PMO materials the use of efficient oxidising agents such as Br_2 or H_2O_2 is not suitable, since the mesoporous structure would be destroyed. Instead, concentrated nitric acid as a mild oxidizing agent (HNO_3) is appropriate.

Finally, further detailed investigations on these functionalised mesoporous materials with respect to their high proton conductivity and water uptake are necessary. Both properties are credited to the mesopores and to the functional groups, which are anchored in the inner pore wall. For that reason, a selective pore opening and closing might shed light on their influence. Thus, a photoresponsive coumarin derivate can be grafted on the pore outlet of proton conducting Si-MCM-41- SO_3H . Irradiation of UV light longer than 310 nm wavelength to this coumarin-modified Si-MCM-41- SO_3H induces the photodimerization of coumarin to close the pore outlet with cyclobutane dimer. As a result these materials should show drastic decreased proton conductivities, since the proton transport through the pore channels is hindered. Irradiation to the dimerized coumarin-modified Si-MCM-41- SO_3H with shorter wavelength UV light around 250 nm regenerates the coumarin monomer derivative by the photocleavage of cyclobutane dimer. Furthermore, a controlled water release and storage in the final composite membrane might be possible.

7 Appendix

Publications Included in the Thesis

1. M. Sharifi, R. Marschall, M. Wilkening, M. Wark, Proton conductivity of ordered mesoporous materials containing aluminium, *J. Power Sources* 195, 2010, 7781-7786.
2. M. Sharifi, R. Marschall, M. Wilhelm, D. Wallacher, M. Wark, Detection of homogeneous distribution of functional groups in mesoporous silica by small angle neutron scattering and in-situ adsorption of nitrogen or water, *Langmuir* 27, 2011, 5516-5522.
3. M. Sharifi, C. Köhler, P. Tölle, T. Frauenheim, M. Wark, Proton conductivity of SO₃H-functionalized benzene-PMO, *Small* 8, 2011, 1086-1097.
4. M. Sharifi, J. Schneider, M. Wark, Investigation on the optimal oxidation agent for a maximum yield of sulfonic acid groups in MCM-41, *Microporous Mesoporous Mater.*, in press Oct. 2011, DOI: 0.1016/j.micromeso.2011.10.008
5. M. Sharifi, M. Wark, D. Freude, J. Hasse, Highly proton conducting sulfonic acid functionalized mesoporous materials studied by impedance spectroscopy, MAS NMR spectroscopy and MAS PFG NMR diffusometry, submitted to *Microporous Mesoporous Mater*, Dec. 2011.
6. M. Sharifi, D. Wallacher, M. Wark, Small angle neutron scattering and in-situ adsorption of nitrogen study on periodic mesoporous organosilica materials, to be submitted *Beilstein Journal of Technology*.

Publications Not Included in the Thesis

1. R. Marschall, M. Sharifi, M. Wark, Proton conductivity of imidazole functionalized ordered mesoporous silica: Influence of type of anchorage, chain length and humidity, *Microporous Mesoporous Mater.* 123, 2009, 21-29.
2. A. Düvel, E. Romanova, M. Sharifi, D. Freude, M. Wark, P. Heitjans, M. Wilkening, Mechanically induced phase transformation of Al₂O₃ into Al₂O₃ Access to structurally disordered-Al₂O₃ with a controllable amount of penta-coordinated Al sites, *J. Phys. Chem.* 115, 2011, 22770-22780.
3. R. Marschall, M. Sharifi, M. Wark, Protonenleitende Komposit-Membranen für zukunftsorientierte Anwendungen in Brennstoffzellen, *Entsalzungsanlagen*

und in der Photokatalyse, Chemie Ingenieur Technik 2011, 83, No. 12, 2177-2187.

4. P. Tölle, C. Köhler, R. Marschall, M. Sharifi, M. Wark and T. Frauenheim, Proton Transport in Functionalised Additives for PEM Fuel Cells: Contributions from Atomistic Simulations, submitted to Chemical Society Reviews (Nov. 2011).

Contributions to Conferences

1. M. Huang, M. Sharifi, R. Marschall, M. Wark, J. Caro, Insight into proton conductivity of ordered mesoporous materials containing aluminium, 21. Deutsche Zeolith-Tagung, Kiel, März 2009, (Talk)
2. M. Sharifi, R. Marschall, M. Wilkening, M. Wark, Proton Conductivity of Ordered Mesoporous Materials Containing Aluminium, MRS Spring Meeting, Straßburg, Frankreich, Juni 2009, (Talk)
3. M. Sharifi, R. Marschall, M. Wark, J. Caro, Insight into proton conductivity of ordered mesoporous materials containing aluminium, 22. Deutsche Zeolith-Tagung, München, März 2010, (Talk)
4. M. Sharifi, D. Wallacher, M. Wark, Investigation of small angle neutron scattering during in-situ adsorption of water in SO₃H-functionalised SiO₂ pore channels, Deutsche Tagung für Forschung mit Synchrotronstrahlung, Neutronen und Ionenstrahlen an Großgeräten, SNI 2010, Berlin, Februar 2010, (Poster)
5. M. Sharifi, R. Marschall, D. Wallacher, M. Wark, Modified ordered mesoporous silica materials with high proton conductivity for fuel cell application, 1st International Conference on Materials for Energy, Karlsruhe, Juni 2010 (Talk)
6. M. Sharifi, D. Wallacher, M. Wark, Proton conductivity of SO₃H-functionalized benzene-PMO, 23. Deutsche Zeolith-Tagung, Erlangen, März 2011, (Poster)
7. M. Sharifi, M. Wark, Improved polymer-membranes with SO₃H-functionalized benzene-periodic mesoporous organosilica, 2011 MRS Fall Meeting, Dezember 2011, Boston (USA), (Talk)

Curriculum Vitae

Personal data

Date of birth	15/06/1983
Place of birth	Kabul, Afghanistan
Nationality	german
Marital status	unmarried, no children

Higher education

Since 03/2009	Gottfried Wilhelm Leibniz University Hannover , Naturwissenschaftliche Fakultät, Submission of the doctoral thesis: “Functionalisation of mesoporous materials for application as additives in high temperature PEM fuel cell membranes”
07/2008-02/2009	Gottfried Wilhelm Leibniz University Hannover , Degree: Diplom-Chemiker Diploma thesis: “Synthesis of Silicamaterials for application Fuel Cell Membranes”
10/2003-06/2008	Gottfried Wilhelm Leibniz University Hannover , Study of chemistry

Education

08/1996-06/2003	Gymnasium Helene-Lange-Schule , Hannover
09/1994-06/1996	Orientierungsstufe OS Birkenschule , Hannover
08/1190-07/1994	Grundschule Goetheplatz , Hannover

Erklärung zu dieser Dissertation

Hiermit erkläre ich, dass ich die vorliegende Dissertationsschrift selbständig verfasst und alle benutzten Hilfsmittel sowie zur Hilfeleistung herangezogene Institutionen vollständig angegeben habe.

Diese Dissertation wurde nicht schon als Diplom- oder ähnliche Prüfungsarbeit verwendet.

Hannover, den